NASA Technical Memorandum 106524

A Continuing Search for a Near-Perfect Numerical Flux Scheme

Part I: AUSM+

Meng-Sing Liou
Lewis Research Center
Cleveland, Ohio

March 1994

National Aeronautics and
Space Administration

A Continuing Search for a Near-Perfect Numerical Flux Scheme

Part I: AUSM+

Meng-Sing Liou
National Aeronautics and Space Administration
Lewis Research Center
Cleveland, Ohio 44135

Abstract

While enjoying demonstrated improvement in accuracy, efficiency, and robustness over existing schemes, the Advection Upstream Splitting Scheme (AUSM)[1,2] has been found to have some deficiencies in extreme cases. This paper describes recent progress towards improving the AUSM while retaining its advantageous features. The new scheme, termed AUSM$^+$, features: (1) Unification of velocity and Mach number splittings reported in [1,2], (2) Exact capture of a single stationary shock, and (3) Improvement in accuracy.

In this paper, we lay out a general construction of the AUSM$^+$ scheme and then focus on the analysis of the scheme and its mathematical properties, heretofore unreported. We prove monotonicity and positivity, and give a CFL-like condition, for first and second order schemes and for generalized curvilinear co-ordinates. Finally, results of numerical tests on many problems are given to confirm the capability and improvements on a variety of problems including those failed by prominent schemes.

1. INTRODUCTION

Seeking an *accurate* numerical scheme for capturing shock and contact discontinuities, with minimal numerical dissipation and oscillations, has been a lasting challenge to the computational fluid dynamicist as well as numerical analyst since the advent of computers. The 1980s witnessed an explosive interest and research in upwind schemes for their capability of achieving high accuracy over a wide range of problems described by Euler or Navier-Stokes equations. Today, upwind schemes undoubtedly have become the main spatial discretization techniques adopted in nearly all major codes.

While much has been said in the literature about the successes and fails of various schemes (see for example a recent survey by Roe [3]), Quirk[4] recently added an interesting catalogue of situations that deny several current Riemann solvers success, serving to

increase the general level of awareness to their limitations. This report will, however, only comment on some of these methods to the extent that is relevant to the motivations and issues concerning the the development of a new flux scheme.

It is well known that upwind schemes are generally classified in two categories, either flux-vector or flux-difference splittings. Flux-vector splittings (FVS) have proved to be a simple and useful technique for arriving at upwind differencing and are pre-eminently suited for use in implicit schemes. The Steger-Warming splitting [5] utilizes the complete wave struture (the eigenvectors of the Jacobian matrix — three waves in 1D Euler equations), and the homogeneous property at a given state. This splitting, achieved by grouping positive and negative eigenvalues, is nondifferentiable and leads to glitches when eigenvalues change sign. Fixes have been proposed to remedy this deficiency, but at the expense of introducing excessive numerical diffusion.

The Van Leer splitting [6] uses only two waves to achieve splitting. The splitting is made to be differentiable and gives accurate solution for many steady and unsteady *inviscid* problems. Our recent experiences, to be reported separately, further reaffirm that the VLS is quite an admirable solver for inviscid problems, in particular those involving strong shocks and their interactions. Unfortunately the intent for making a smoother transition at the sonic points brings an unacceptable amount of diffusion at low speed, attaining maximum error at $M = 0$. As a result, the boundary layer which has nearly vanishing transverse velocity is significantly broadened, yielding incorrect pressure and temperature distributions [1,7]. Owing to the same cause, significant error also appears for stationary or slowly moving contact discontinuity. (See Fig. 5.) A strategy for eliminating the above diffusion has been proposed in [8] in which each mass flux component is made to vanish as $|M| = 0$. This, however, turns out to be too strong a requirement for designing numerical fluxes — a serious stability problem crops up.

Flux difference splittings (FDS) are generally acknowledged to be accurate for both Euler and Navier-Stokes calculations, although they are substantially more expensive than the FVS to compute. The Roe splitting [9] perhaps is most popular of the FDS; nearly every major code offers an option to use the Roe splitting in one form or another. A major complaint about the Roe scheme is its need to inject an entropy fix to eliminate certain nonphysical solutions. Unfortunately this fix should be tuned between problems, inevitably introducing superfluous diffusivity to the viscous solution in exchange for stability. In addition to the failings catalogued by Quirk[4], the Roe splitting is found to be unstable for unsteady rarefaction-rarefaction waves.

The Osher-Soloman splitting [10], save its entropy-satisfying property, is found not totally immune from difficulties. Its solution may be path-dependent on the natural or reverse order chosen. One example where the Osher-Solomon scheme fails is again the blunt body problem where the natural order is found to yield an anomalous solution, although different from Roe's solution.

A first glance of the above summary may suggest a bleak conflict — the simplicity of the FVS comes at a price of reduced accuracy due to numerical diffusion, while the

FDS attains increased accuracy at a cost of decreased efficiency. The current research is motivated by the desire to combine the efficiency of FVS and the accuracy of FDS to arrive at ways that do away with the problem of numerical diffusion with only a small (if any) increase in complexity. To be practically useful, such a scheme should hold robustness/stability, in addition to accuracy and efficiency, for a *wide* range of problems — Euler and Navier-Stokes equations, ideal and nonequilibrium gass, and steady and unsteady flows. Our recent attempts towards deriving a scheme meeting these goals have proven to be quite fruitful, resulting in so-called the AUSM [1,2] and its derivatives such as AUSMDV [11] and the present AUSM$^+$, and the HUS [12,13]. Both AUSMs and HUS are based upon rather different design concepts and the latter, reported earlier in [12,13] by Coquel and Liou, will be further elaborated with a much detailed theoretical development and construction in a forthcoming paper [14]. Another product deserving serious attention as well is called AUSMDV and is given with full details in [11]. The present paper is a complement to the above research, but addresses different topics of interest.

Several efforts have been attempted to improve the original Van Leer scheme, in particular by Hänel et al [15,16]. Van Leer, recently based on their approach [16], has made a significant improvement [17], in which the temperature distribution of a hypersonic conic flow is predicted accurately. Unfortunately, pressure glitch is observed in the calculation. Thus, the effort for searching improved numerical flux functions is still continuing, striving for the goal of arriving towards the so-called "ultimate" scheme.

Unlike the conventional flux schemes such as flux-vector and flux-difference splittings, we begin the development of the AUSM schemes by separating the convective and pressure fluxes. Appropriate polynomial functions for the *nonlinear* waves ($(u \pm a)$ in 1D case) are used to represent their interactions, leading to representations of the convective velocity and the pressure at the cell interface. Finally the scalar quantity $(\rho, \rho u, \rho H)$ at the upwind location is properly advected by this interface velocity, hence the scheme is coined as the Advection Upstream Splitting Method, AUSM for short. The new flux scheme has been shown to yield improved accuracy, efficiency, and robustness by us and independently by others.

Most recently, the notion of this splitting procedure has been adopted by several authors [18,19] for various motivations. Jameson [18] rewrote the splitting in the form of artificial dissipation for the central-differencing setting and chose a different set of polynomial representations for splitting M and p. Unfortunately, an adjustable and problem-dependent constant has been inserted in the formula, thereby reverting back to complaints that upwind differencing is meant to avoid. For usual problems, a nonvanishing constant has to be set, leading to excessive smearing in both contact and shock discontinuities. Halt and Agarwal [19] have experimented with a variant in which the pressure work term is separated out from the total enthalpy, as first proposed by Steger [5,20]. The immediate drawback of doing this is that the total enthalpy is no longer guaranteed to be conserved when the situation so demands (see cases and related results in [21]). The conservation of total enthalpy, not only having theoretical justification, is also proved to be critical

in viscous calculations. Indeed, this is the very idea of Hänel [15] for retaining the total enthalpy in Van Leer's FVS.

Even as the original scheme AUSM enjoys remarkable success, its drawbacks also surface. In a continuing search for a near-perfect (if it exists) numerical flux scheme, we report in this paper a recent progress towards this end. We aim at deriving an improved flux formula by addressing some fundamental properties by way of rigorous mathematical derivation. Consequently, this new-revised scheme, termed AUSM$^+$, can be shown either analytically or numerically, to satisfy the following properties: (1) Exact resolution of a single stationary normal shock or contact discontinuity, (2) Positivity condition, and (3) Entropy condition. Property (1) is important not only in shock resolution of inviscid flows, but also in boundary/shear-layer resolution of viscous flows. Property (2) proves to be closely related to the robustness of the scheme for high speed flows and species calculation. And property (3) selects the physically correct solution by rejecting the expansion shocks. While these are desirable properties, none of the existing schemes are known to possess all of them. For example, properties (2) and (3) are violated by the Roe splitting, and (1) and (2) by the Osher splitting. In practice, some "fixes", of little mathematical or physical justification, have been inserted to prevent the scheme from failing. In the case of the Roe scheme, a heavy dose of entropy fix can be prescribed to cure the "carbuncle" phenomena, which is believed to be caused primarily by its failure to satisfy property (3).

Like its predecessor, the AUSM$^+$ is simple conceptually with close connection to physical interpretation; it is also simple algebraically, leading to greater computational efficiency, for it requires only $O(n)$ operations for evaluating fluxes, n being the dimension of the flux.

In this paper, we will give the details of the development and analysis of the AUSM$^+$ scheme for ideal-gas flows. In a separate paper [21], we will include non-equilibrium flows. This paper is organized as follows. In section 2 we give a detalied derivation of the proposed scheme and prove some relevant properties. In section 3 we analyze the numerical flux developed in the previous section and compare it with other flux schemes. Also we present proof of monotonicity and positivity, and the associated CFL-like condition. In section 4 we give formulas for extension to higher-order accuracy and present similar proofs as in section 3. In section 5 an extention to the generalized curvilinear coordinates is given. In section 6 we discuss the boundary conditions used in the calculations. Test cases are shown in section 7 together with discussion and comparisons with other schemes. Finally we conclude the paper with a brief remark.

2. FORMULATION

Consider as an initial-value problem the one-dimensional system of conservation laws

for ideal-gas flows:

$$\begin{aligned} &\frac{\partial \mathbf{U}}{\partial t} + \frac{\partial \mathbf{F}}{\partial x} = 0, \qquad t > 0, \quad -\infty \le x \le \infty, \\ &\mathbf{U}(x,0) = \mathbf{U}_0(x), \end{aligned} \tag{1}$$

where $\mathbf{U} = (\rho, \rho u, \rho e_t)^T$ belongs to a phase space $\mathcal{U} \in \mathcal{R}^p$, the inviscid flux $\mathbf{F} = (\rho u, \rho u^2 + p, \rho u h_t)^T$ denotes a smooth mapping $\mathbf{F} : \mathcal{U} \to \mathcal{R}^p$, and the specific total energy $e_t = e + u^2/2 = h_t - p/\rho$.

For the numerical solution of (1), we shall consider piecewise constant approximations $\mathbf{U}_j^{n+1}$ defined by the explicit 3-point scheme in conservation form

$$\mathbf{U}_j^{n+1} = \mathbf{U}_j^n - \lambda(\mathbf{F}_{j+1/2}^n - \mathbf{F}_{j-1/2}^n), \quad n \in N,\ j \in Z, \tag{2}$$

where $\lambda = \Delta t/\Delta x$, Δt and Δx being respectively the time and space steps. Here, the numerical flux defined by

$$\mathbf{F}_{j+1/2}^n = \mathbf{F}_{j+1/2}(\mathbf{U}_j^n, \mathbf{U}_{j+1}^n), \ \S \quad \mathcal{U} \times \mathcal{U} \to \mathcal{U} \in \mathcal{R}^p, \tag{3}$$

is assumed to be a Lipschitz continuous function and satisfy the consistency condition:

$$\mathbf{F}_{j+1/2}(\mathbf{U}_j, \mathbf{U}_j) = \mathbf{F}(\mathbf{U}_j). \tag{4}$$

In the finite-volume formulation (2)-(3), the differences among all numerical schemes lie essentially in the definition of the numerical flux $\mathbf{F}_{j+1/2}$ evaluated at the cell interface. It is obvious that different numerical fluxes will satisfy different sets of criteria such as positivity, entropy condition, differentiability, etc. and are expected to yield various degrees of satisfaction in performance.

As a first step in the formulation of the AUSM family of schemes, we recognize the convection and acoustic waves as two physically distinct processes, and write the inviscid flux as a sum of the convective and pressure terms:

$$\mathbf{F} = \mathbf{F}^{(c)} + \mathbf{P}, \tag{5a}$$

where

$$\mathbf{F}^{(c)} = c\mathbf{\Phi} = \begin{cases} u \begin{pmatrix} \rho \\ \rho u \\ \rho h_t \end{pmatrix}, & \text{if } c = u \\ M \begin{pmatrix} \rho a \\ \rho u a \\ \rho h_t a \end{pmatrix}, & \text{if } c = M, \end{cases} \tag{5b}$$

§ In this paper we always use the half-integer subscripts "$j + 1/2$", $j \in Z$, to denote "numerical" function $f : \mathcal{U} \times \mathcal{U} \to \mathcal{U} \in \mathcal{R}^p$. It should not be confused with a variable having an integer subscript "j", which indicates a function $f : \mathcal{U} \to \mathcal{U} \in \mathcal{R}^p$.

and

$$\mathbf{P} = \begin{pmatrix} 0 \\ p \\ 0 \end{pmatrix}. \tag{5c}$$

Here the convective flux $\mathbf{F}^{(c)}$ contains the passive scalar quantities in $\mathbf{\Phi}$ convected by the velocity c. Depending on whether the convective speed c is chosen to be either u or M, the vector $\mathbf{\Phi}$ has the corresponding contents. The pressure flux $\mathbf{P}$ contains solely the pressure term.

One immediate question to be posed is which of the two convective speed formulas, respectively referred to as the U- and M-splittings, is preferred. In [2], we stated that the U-splitting was found to be more robust than the M-splitting for the shock-tube problem since a larger time step is allowed at start, while solutions for several other test problems gave no significant differences. On the other hand, the former smears the stationary contact discontinuity since the interface velocity does not vanish, while the latter holds the contact discontinuity exactly. This ambiguity actually suggests that a unified formula should be pursued, which indeed leads to a major discovery in our continuing effort towards improving the numerical flux. The net result is a unified formula that in addition leads to an exact capturing of a single stationary shock. Moreover, due to a judicious choice of a common speed of sound for defining the interface Mach number, the new numerical flux can give rise to an exact capture of a single stationary shock.

As a preliminary, we shall express the *numerical convective flux* $\mathbf{F}^{(c)}_{j+1/2}$ at the interface $j+1/2$ straddling the j-th and $(j+1)$-th cells as

$$\mathbf{F}^{(c)}_{j+1/2} = M_{j+1/2}\mathbf{\Phi}_{j+1/2}. \tag{6}$$

We stress now that, as will be seen later, it is immaterial in our development whether we write it in terms of u or M for the unified formula. As the M-splitting may be more familiar, we will adopt it in this section and change to the U-splitting in the next section for a cleaner algebraic manipulation.

To define the numerical fluxes, two steps are taken. First, we define the interface velocity and pressure by considering the *nonlinear* fields. Mathematically, we propose to separately deal with the genuinely *nonlinear* fields $(u+a, u-a)$ and the *linearly* degenerate field (u). In this approach, the coupling between velocity and pressure, as described by the characteristic relationships, is honored via the genuinely nonlinear fields, which will be described in detail in §2.2. In the sequel we respectively give detailed formulas for the major elements involved in $\mathbf{F}_{j+1/2}$: (1) definition of $\mathbf{\Phi}_{j+1/2}$, (2) definition of $(M_{j+1/2}, P_{j+1/2})$, and (3) definition of $a_{j+1/2}$.

2.1 Definition of $\mathbf{\Phi}_{j+1/2}$

The scalar quantities in $\Phi_{j+1/2}$ are convected by the *linear* field via the interface velocity $M_{j+1/2}$ using a simple upwinding:

$$\Phi_{j+1/2} = \begin{cases} \Phi_j, & \text{if } M_{j+1/2} \geq 0, \\ \Phi_{j+1}, & \text{otherwise.} \end{cases} \tag{7}$$

2.2 Definition of $(M_{j+1/2}, p_{j+1/2})$

Anticipating contributions from "j" and "$j+1$" states to the interface Mach number $M_{j+1/2}$, let us write the mapping $m : \mathcal{U} \times \mathcal{U} \to \mathcal{U} \in \mathcal{R}$,

$$M_{j+1/2} = m(M_j, M_{j+1}). \tag{8a}$$

Specifically we write $M_{j+1/2}$ as a sum of two individual components,

$$M_{j+1/2} = M_j^+ + M_{j+1}^-, \tag{8b}$$

where the superscripts "+" and "–" are understood to be associated with the right- and left-running waves.

For 1D conservation laws, the nonlinear characteristic equations are:

$$dp \pm \rho a du = 0, \quad \text{along} \quad \frac{dx}{dt} = u \pm a. \tag{9}$$

This simply suggests that the velocity and pressure are closely coupled and both quantities may be thought of propagating locally at the speeds $u \pm a$. For $|M| < 1$, the two waves move in the opposite directions and interact with each other. Hence the interface velocity and pressure, composed of the interaction of these two waves, are constructed using $(u \pm a)$ as basis functions for polynomial expansions. This suggests the following expansion in terms of $(M \pm 1)$:

$$M^{\pm} = \frac{1}{2}(M \pm 1), \quad \text{for } |M| < 1. \tag{10}$$

This in fact is a form of eigenvalue expansion, just utilizing the genuinely nonlinear fields. Then from (8b), the interface Mach number is defined, as $|M| < 1$, by

$$M_{j+1/2} = \frac{1}{2}[(M+1)_j + (M-1)_{j+1}]. \tag{11}$$

Note that as in Van Leer's splitting, the present method heavily makes explicit use of the eigenvalues of the nolinear wave, $M \pm 1$. Using the eigenvalues as a basis for expressing the numerical fluxes is quite common in the upwind formulation. For example, it comes

naturally in the Steger-Warming and Roe fluxes as the Jacobian matrix is explicitly expressible in terms of its eigenvalues. Specifically, Steger-Warming splitting [5] begins by grouping $\mathbf{F}$ as:

$$\mathbf{F} = \frac{\rho}{2\gamma}\left\{(u+a)\begin{pmatrix}1\\ u+a\\ H+ua\end{pmatrix} + (u-a)\begin{pmatrix}1\\ u-a\\ H-ua\end{pmatrix} + 2(\gamma-1)u\begin{pmatrix}1\\ u\\ u^2/2\end{pmatrix}\right\}. \qquad (12)$$

To remove non-differentiability of (10) when sign changes, Van Leer [6] chose differentiable, second-order polynomials:

$$M^{\pm} = \pm\frac{1}{4}(M \pm 1)^2. \qquad (13)$$

It is evident that the above split formula (13) results in an unsymmetric distribution of signals propagated by the characteristic speeds $(M \pm 1)$ as $M \neq 0$ and becomes the simple (symmetric) average as M tends to zero, leading to the formula used commonly in the pressure-based codes for incompressible flows.

In the present study, we present a more general footing for designing the split formulas. First we introduce the following:

Proposition 2.1: Let the respective split Mach numbers $M^{\pm}$ be chosen such that they hold the following properties:

[M1]: $M^+ + M^- = M$, for consistency.
[M2]: $M^+ \geq 0$ and $M^- \leq 0$.
[M3]: $M^{\pm}$ are monotone increasing functions of M.
[M4]: $M^+(M) = -M^-(-M)$, i.e., a symmetry property.
[M5]: $M^+ = M$ as $M > 1$; $M^- = M$ as $M < -1$.
[M6]: $M^{\pm}$ are continuously differentiable.

Consequently we assert the following necessary results.

Lemma 2.1: $M_{j+1/2} \in [M_j, M_{j+1}], \quad j \in Z.$

Proof. Let $D = (M_{j+1/2} - M_j)(M_{j+1/2} - M_{j+1})$, substituting (8*b*) and [M1] in D gives

$$D = -(M_j^- - M_{j+1}^-)(M_j^+ - M_{j+1}^+) \leq 0$$

where the product of two parentheses is nonnegative by virtue of [M3].

Remark: Owing to [M2], [M3], and [M5], it is easy to see $0 < M^+ < 1$ and $0 > M^- > -1$ as $|M| < 1$.

Definition of M: The split Mach numbers given as below,

$$M^{\pm} = \begin{cases} \frac{1}{2}(M \pm |M|), & \text{if } |M| \geq 1, \\ M_\beta^{\pm}(M), & \text{otherwise,} \end{cases} \qquad (14a)$$

where

$$M_\beta^\pm(M) = \pm\frac{1}{4}(M \pm 1)^2 \pm \beta(M^2-1)^2, \tag{14b}$$

satisfy the properties [M1]-[M6]. $M^\pm_{\beta=0}$ reduces to the Van Leer formula [6] and is the lowest degree polynomial continuous at $M = \pm 1$. Figure 1 displays the distribution of $M^\pm$ with various values of β.

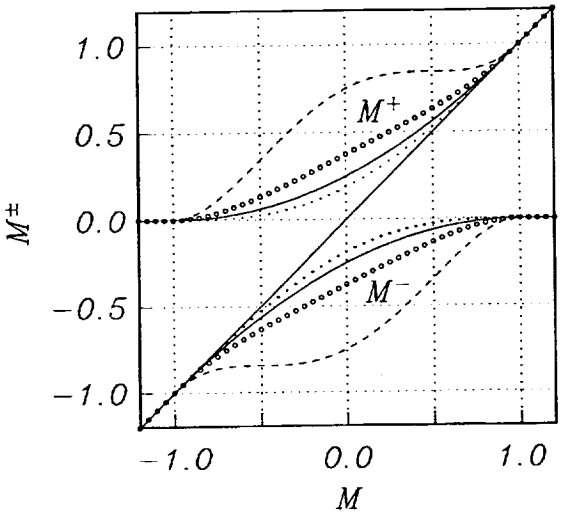

Fig. 1 $M^\pm_\beta$ vs M; solid line: $\beta = 0, \cdots : \beta = -1/16, -- : \beta = 1/2, \text{oo} : \beta = 1/8$.

Let

$$M^\pm_{j+1/2} = \frac{1}{2}(M_{j+1/2} \pm |M_{j+1/2}|) = \frac{1}{2}M_{j+1/2}(1 + \text{sign}(M_{j+1/2})), \text{ §} \tag{15}$$

combining (6), (7), and (15) gives

$$\mathbf{F}^{(c)}_{j+1/2} = M^+_{j+1/2}\mathbf{\Phi}_j + M^-_{j+1/2}\mathbf{\Phi}_{j+1}. \tag{16}$$

Note that as $M_{j+1/2}$ is identically equal to zero, the sign of $M_{j+1/2}$ is immaterial since the convective flux vanishes with $M_{j+1/2}$. This also means the switching is continuous, but not differentiable.

We remind the reader that the Mach numbers appearing in (13)-(14) need *not* be based on the speed of sound at grid $a_j, j \in Z$. In fact we propose in this paper to use a general interface value $a_{j+1/2}$, which will be determined in §2.3 to achieve some unique property.

§ We caution the reader that here the " $\pm$ " signs in the *interface* Mach number have different meanings than that attached to the cell-point definitions in (14a,b).

We turn now to the pressure splitting in which the interface pressure is defined by

$$p_{j+1/2} = p_j^+ p_j + p_{j+1}^- p_{j+1}. \tag{17}$$

Noting that we propose the use of normalized split pressure polynomials $p^\pm : M \in \mathcal{R} \to p^\pm(M)[0,1]$. First observed in reference [22], the pressure can be expanded using the same set of basis functions, $(M \pm 1)$, as clearly implied from the characteristic equations (9).

Proposition 2.2: We require that the split pressures $p^\pm$ satisfy the following properties:

[P1] $p^+ + p^- = 1$, for consistency.
[P2] $0 \le p^\pm \le 1$, as required by the physical constraint that the pressure be nonnegative.
[P3] p^+ is a monotone increasing function of M, but p^- monotone decreasing with M, thereby allowing proper transition for upwinding.
[P4] $p^+(M) = p^-(-M)$
[P5] $p^+ = 1$ as $M > 1$; $p^- = 1$ as $M < -1$.
[P6] $p^\pm$ are continuously differentiable.

Similar assertion can be made about the pressure splitting as for the Mach number. We now prove the following properties for $p_{j+1/2}$.

Lemma 2.2: $p_{j+1/2} \in [0, p_j + p_{j+1}]$.
Proof. The proof follows directly by virtue of [P2] and $0 \le \frac{1}{2}(1 \pm \text{sign}(M)) \le 1$.

Remark: One can also show that $p_{j+1/2}$ is a monotone function of both p_j and p_{j+1}, and monotone increasing in M_j but decreasing in M_{j+1} due to requirement [P3].

Definition of P: The split pressures given below,

$$p^\pm = \begin{cases} \frac{1}{2}(1 \pm \text{sign}(M)), & \text{if } |M| \ge 1, \\ p_\alpha^\pm(M), & \text{otherwise.} \end{cases} \tag{18a}$$

where

$$p_\alpha^\pm(M) = \frac{1}{4}(M \pm 1)^2(2 \mp M) \pm \alpha M(M^2 - 1)^2, \tag{18b}$$

hold [P1]-[P6]. Clearly, $p_{\alpha=0}^\pm$, corresponding to Van Leer's formula, are the lowest degree

differentiable polynomials satisfying [P1]-[P6]. The $p_\alpha^\pm$ vs M curves are shown in Fig. 2.

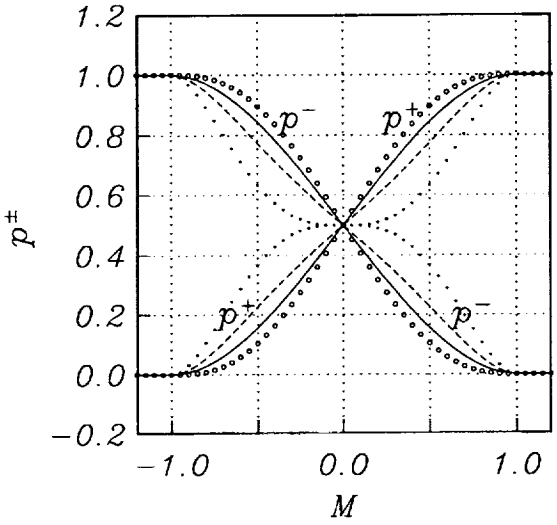

Fig. 2 $p_\alpha^\pm$ vs M; solid line: $\alpha = 0, \cdots : \alpha = -3/4, -- : \alpha = -1/4, \circ\circ : \alpha = 3/16$.

Next we suggest the values of parameters (α, β) to be used.

Lemma 2.3: To satisfy properties [M1]-[M6] and [P1]-[P6], we have

$$-3/4 \leq \alpha \leq 3/16, \tag{19a}$$

$$-1/16 \leq \beta \leq 1/2. \tag{19b}$$

Proof. The proof is simple and omitted here.

Lemma 2.4: The parameters (α, β) selected on the basis of the criteria:

$$\frac{d^2 M_\beta^\pm}{dM^2}(0) = 0, \tag{20a}$$

and

$$\frac{d^2 p_\alpha^\pm}{dM^2}(\pm 1) = 0, \tag{20b}$$

are

$$\alpha = 3/16 \quad \text{and} \quad \beta = 1/8. \tag{21}$$

Proof. The proof is trivial and omitted here.

The curves corresponding to these values are included in Figs. 1 and 2 respectively. These values are recommended for use as this pair have given the best performance over many problems tested [21], including those shown in the present paper.

Lemma 2.5: Given a bounded set K of $\mathcal{U}$, then for every states (M_L, M_R) and $(\tilde{M}_L, \tilde{M}_R)$ in K, there exists constants $C^{\pm}(\beta) > 0$ and $C^{\pm}(\alpha) > 0$, such that

$$|M_L^+ - \tilde{M}_L^+| \leq C^+(\beta)|M_L - \tilde{M}_L|, \tag{22a}$$
$$|M_R^- - \tilde{M}_R^-| \leq C^-(\beta)|M_R - \tilde{M}_R|. \tag{22b}$$

Similarly,

$$|p_L^+ - \tilde{p}_L^+| \leq C^+(\alpha)|M_L - \tilde{M}_L| \tag{23a}$$
$$|p_R^- - \tilde{p}_R^-| \leq C^-(\alpha)|M_R - \tilde{M}_R|. \tag{23b}$$

Proof. Referring to Fig. 1, we make use of the differentiability of $M^{\pm}$ in (14). Setting

$$C^+(\beta) = \max_{M \in \mathcal{R}} |\frac{dM^+}{dM}|,$$
$$C^-(\beta) = \max_{M \in \mathcal{R}} |\frac{dM^-}{dM}|$$

completes the proof. The proof for (23a,b) follows the same steps.

Remark: Under (19b) in **Lemma 2.3**, namely $-1/16 \leq \beta \leq 1/2$, one easily gets $C^{\pm} = 1$.

Lemma 2.6: The interface Mach number defined in (8a,b),

$$M_{LR} = m(M_L, M_R) = M_L^+ + M_R^-,$$

is a Lipschitz continuous function of its arguments and satisfies the consistency condition

$$m(M, M) = M.$$

It is monotone nondecreasing in its first argument, nonincreasing in its second.

Proof. The proof for Lipschitz continuity is equivalent to showing for every states (M_L, M_R) and $(\tilde{M}_L, \tilde{M}_R)$ in K of $\mathcal{U}$ that

$$\begin{aligned} |m(M_L, M_R) - m(\tilde{M}_L, \tilde{M}_R)| &= |M_L^+ + M_R^- - \tilde{M}_L^+ - \tilde{M}_R^-| \\ &= |(M_L^+ - \tilde{M}_L^+) + (M_R^- - \tilde{M}_R^-)| \\ &\leq |(M_L - \tilde{M}_L| + |M_R - \tilde{M}_R|. \end{aligned}$$

The proof of consistency and monotone property is straightforward and omitted.

Remark: One can assume in general for higher-order formulas that

$$M_{j+1/2} = m(M_{j-k+1}, ..., M_{j+k}),$$

and similarly

$$p_{j+1/2} = p(M_{j-k+1}, ..., M_{j+k}; p_{j-k+1}, ..., p_{j+k}),$$

for $k \geq 1$ and show the Lipschitz continuity and consistency condition.

2.3 Definition of $a_{j+1/2}$

Recall that we still have one yet unattended task: namely selecting an interface speed of sound $a_{j+1/2}$ in order to achieve the unified formula for both the U- and M-splittings. To achieve this unification, it is obvious we can no longer use each respective speed of sound, a_j or a_{j+1}, but instead should use a common one:

$$a_{j+1/2} = a(\mathbf{U}_j, \mathbf{U}_{j+1}). \tag{24}$$

In other words, the interface Mach number should be defined on the basis of a properly defined speed of sound. Since the interface flux is viewed as a recipient of contributions from both neighboring cells, it makes sense to use a common speed of sound evaluated there, as a basis for determining upwinding. It is this freedom that allows us to make a favorable choice to attain an exact capture of a single stationary shock. This concept of using a common speed of sound is also employed in [11].

Lemma 2.6: Consider a stationary shock problem:

$$\mathbf{U} = \begin{cases} \mathbf{U}_L, & x \leq x_j, \\ \mathbf{U}_R, & x > x_j, \end{cases}$$

where the normal shock relation is connected by $\mathbf{U}_L$ and $\mathbf{U}_R$ and $u_j > a_j$. Let a_j^* be the critical speed of sound evaluated at $\mathbf{U}_j (= \mathbf{U}_L)$, then

$$a_{j+1/2} = a_j^{*2}/u_j \tag{25}$$

exactly captures the shock without any intermediate states.

Proof. Referring to Fig. 3, we consider at most one intermediate (numerical) state "i" between the "L" and "R" states.

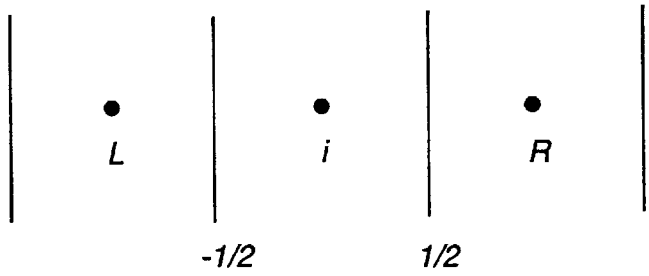

Fig. 3 One intermediate shock cell between "L" and "R".

Let us now express the numerical flux at interfaces (denoted here respectively by $\mp 1/2$) enclosing the intermediate cell i. In order to explicitly include the undefined speed of sound, we opt for using the velocity (U-) splitting. Similar to (8b) and (14a,b), (or referring to [2],) we write

$$u_{-1/2} = u_L^+ + u_i^-.$$

Assuming $M_L > 1$ and $M_i < 1$ without loss of generality, (since there must be a subsonic point connecting the supersonic point in the case of normal shock) then we have

$$u_{-1/2} = u_L - (u_i - a_{-1/2})^2 g^+(u_i, a_{-1/2}),$$

where we define

$$g^{\pm}(u,a) = \frac{1}{4a}(1 + 4\beta(\frac{u}{a} \pm 1)^2).$$

It is easy to show $u_{-1/2} > 0$ as $u_L > u_i$, hence by (16) we get

$$\mathbf{F}_{-1/2} = \begin{pmatrix} m_{-1/2} \\ u_L m_{-1/2} + p_{-1/2} \\ h_{tL} m_{-1/2} \end{pmatrix}, \qquad m_{-1/2} = \rho_L u_{-1/2}.$$

This flux must be balanced with $\mathbf{F}_L$ as the "L" state is fixed. Hence, a simple algebra yields

$$\begin{pmatrix} u_{-1/2} \\ p_{-1/2} \end{pmatrix} = \begin{pmatrix} u_L \\ p_L \end{pmatrix}.$$

These two conditions can be satisfied exactly, for any (ρ_i, p_i), by requiring only one condition:

$$u_i = a_{-1/2}. \tag{26}$$

Let us now turn to the "1/2" face. The interface velocity becomes

$$u_{1/2} = (u_i + a_{1/2})^2 g^-(u_i, a_{1/2}) - (u_R - a_{1/2})^2 g^+(u_R, a_{1/2}) > 0.$$

The inequality holds as $u_i > u_R$ is expected. Again using (16) yields

$$\mathbf{F}_{1/2} = \begin{pmatrix} m_{1/2} \\ u_i m_{1/2} + p_{1/2} \\ h_{ti} m_{1/2} \end{pmatrix}, \qquad m_{1/2} = \rho_i u_{1/2}.$$

In order to eliminate this intermediate state, we let

$$\mathbf{U}_i = \mathbf{U}_R, \qquad \text{or} \qquad \begin{pmatrix} u_i \\ \rho_i \\ p_i \end{pmatrix} = \begin{pmatrix} u_R \\ \rho_R \\ p_R \end{pmatrix}.$$

It turns out that the last two requirements in the above equation respectively for ρ_i and p_i are automatically satisfied if (26) and the first requirement, $u_R = u_i$, are set. Thus,

$$a_{-1/2} = u_R = u_i.$$

This requirement in fact enforces the conservation of fluxes by relating the upstream supersonic "L" state to the downstream subsonic "R" state. It is desirable to express $a_{-1/2}$ in terms of the upstream state "L". In fact, the well-known Prandtl relation (see for example [23]) is at hand for use.

$$u_R u_L = a_L^{*\,2} = a_R^{*\,2} = \frac{2}{\gamma+1} a_t^2$$

where a_t is the speed of sound based on the total enthalpy h_t. Putting $L \to j$ and $R \to j+1$, we complete the proof.

Remark: It is well known that insofar as determining whether an isoenergetic flow lies at the sonic or in the supersonic or subsonic regime, the critical speed of sound defined above can be used as a reference [23].

Note that the formula (25) is valid for $u_L > a_L^*$. For a flow covering different speed regimes, we extend the definition to:

$$a_{j+1/2} = \min(\tilde{a}_L, \tilde{a}_R), \quad \tilde{a} = a^* \min(1, \frac{a^*}{|u|}). \tag{27}$$

That is, $\tilde{a}$ is taken to be a^* when $|u| < a^*$.

Remark: Other formulas can be also used for simplicity, but at the expense of losing the above exact property. We have tested the following obvious alternatives:

$$a_{j+1/2} = \frac{1}{2}(a_j + a_{j+1}),$$

$$a_{j+1/2} = \sqrt{a_j a_{j+1}},$$

$$a_{j+1/2} = \min(a_j, a_{j+1}).$$

Despite some expected minor differences among their solutions, no other adverse effects have been discovered thus far in our tests.

Remark: The above exact shock capturing property holds for any (α, β).

Remark: The Van Leer splitting modified by the above procedure also allows exact resolution of a shock, see later in Fig. 5.

Remark: Due to the above exact property, the AUSM$^+$, like the Roe splitting, also can not distinguish whether the discontinuity is a shock or an expansion. However, it must be noted that except in this rather isolated situation, the AUSM$^+$ does not behave like the

Roe scheme in other cases where the latter is known to yield unsatisfactory solutions. (See examples 6 and 7 in section 7.) More specifically, the AUSM$^+$, based on our numerical experiences, does not appear to branch into an entropy-violating solution if the initial condition is not exactly the expansion-jump condition.

In summary, the above splittings for both the advective and pressure terms completely define the Euler numerical flux. The AUSM$^+$ algorithm can be simply summarized as follows:

Let j and $j+1$ states be given, then

(1): $M_j = u_j/a_{j+1/2}$, and $M_j = u_{j+1}/a_{j+1/2}$ via (27),

(2): $M_{j+1/2} = M_j^+ + M_{j+1}^-$, and $p_{j+1/2} = p_j^+ p_j + p_{j+1}^- p_{j+1}$,

(3): Get $M_{j+1/2}^{\pm}$ via (15) and

$$\mathbf{F}_{j+1/2} = a_{j+1/2} \left\{ M_{j+1/2}^+ \begin{pmatrix} \rho \\ \rho u \\ \rho h_t \end{pmatrix}_j + M_{j+1/2}^- \begin{pmatrix} \rho \\ \rho u \\ \rho h_t \end{pmatrix}_{j+1} \right\} + \mathbf{P}_{j+1/2}$$

3. ANALYSIS OF AUSM$^+$

Definition 3.1: The numerical flux defined above is rewritten as,

$$\mathbf{F}_{j+1/2} = M_{j+1/2} \frac{1}{2}(\mathbf{\Phi}_j + \mathbf{\Phi}_{j+1}) - \frac{1}{2}|M_{j+1/2}| \Delta_{j+1/2} \mathbf{\Phi} + \mathbf{P}_{j+1/2}, \tag{28}$$

where $(M, p)_{j+1/2}$ are defined in sections 2.2 and 2.3, and $\Delta_{j+1/2}\{\bullet\} = \{\bullet\}_{j+1} - \{\bullet\}_j$.

While the associated properties of the interface quantities $(M, p, a)_{j+1/2}$ have been discussed in the last section, we will address in what follows the mathematical consequences of the complete flux formula (28).

Remark: The first term on the RHS is clearly not a simple average of "j" and "$j+1$" states, but rather a Mach number-weighted average.

Remark: The dissipation coefficient $|M_{j+1/2}|$ is merely a scalar — hence the system is decoupled after $M_{j+1/2}$ has been defined, thus requiring only $O(n)$ operations, in contrast to $O(n^2)$ operations by the other FDS.

Remark: The present scheme does not involve differentiation, specifically the Jacobian matrix, in the evaluation of $\mathbf{F}_{j+1/2}$; it always involves only the common term $M_{j+1/2}$ for any additional conservation laws. Hence, it is readily extendable to a general equation of state and non-equilibrium flows. Again, the cost is only linearly increased with the additional conservation equations considered. In the case of the Roe or Osher scheme in which the Jacobian matrix is essential, there is a need for redefining the averaged/intermediate states as additional equations are included.

We now proceed to prove some interesting numerical properties of the present scheme. For the sake of algebraic clarity, we choose to use variable u, instead of M, in the analysis. Recall that they are interchangeable, for $j \in Z$,

$$u^{\pm}_{j+1/2} = M^{\pm}_{j+1/2} a_{j+1/2}.$$

Lemma 3.1: The present splitting preserves stationary contact discontinuity.

Proof. Let $p_j = p_{j+1} = p$, $u_j = u_{j+1} = 0$, and $\rho_j \neq \rho_{j+1}$ across the stationary contact. Then $M_{j+1/2} = 0$, $p_{j+1/2} = p$, and hence $\mathbf{F}^{(c)}_{j+1/2} = 0$. That is, no non-vanishing numerical convective flux is created at the interface. Hence, the flow remains stationary and the contact discontinuous.

Lemma 3.2: For steady flows, the present scheme preserves the constancy of total enthalpy.

Proof. Assuming without loss of generality a unidirectional flow, e.g., $u > 0$, the discrete continuity equation yields for steady flow,

$$u^{+}_{j+1/2}\rho_j - u^{+}_{j-1/2}\rho_{j-1} = 0.$$

And the energy equation gives

$$u^{+}_{j+1/2}\rho_j h_{tj} - u^{+}_{j-1/2}\rho_{j-1} h_{tj-1} = 0.$$

Hence, we find $h_{tj} = h_{tj-1} = \cdots = h_{t0}$, and the proof is complete.

We note that this property is not satisfied by many upwind schemes, including those by Godunov, Roe, Osher, Steger-Warming, and Van Leer. To my knowledge, only those which upwind the unsplit form of the total enthalpy will preserve this quantity [1,2,11,15-17].

Lemma 3.3: Under the CFL-like condition,

$$0 \leq \lambda\left[u^{+}_{j+1/2} + (-u^{-}_{j-1/2})\right] \leq 1, \quad \lambda = \Delta t/\Delta x, \tag{29}$$

then (a) the density function is monotone, and (b) the scheme preserves positivity of density.

Proof. The mass conservation yields for $j \in Z$,

$$\rho^{n+1}_j = \rho^n_j - \lambda\left(f^n_{\rho,j+1/2} - f^n_{\rho,j-1/2}\right), \quad f_\rho = \rho u, \tag{30a}$$

where

$$f^n_{\rho,j+1/2} = u^+_{j+1/2}\rho^n_j + u^-_{j+1/2}\rho^n_{j+1}.$$

Substituting and rewriting,

$$\begin{aligned}\rho^{n+1}_j &= \lambda u^+_{j-1/2}\rho^n_{j-1} + \left[1 - \lambda(u^+_{j+1/2} - u^-_{j-1/2})\right]\rho^n_j + (-\lambda u^-_{j+1/2})\rho^n_{j+1} \\ &= f(\rho^n_{j-1}, \rho^n_j, \rho^n_{j+1}; u_{j-1/2}, u_{j+1/2}). \end{aligned} \tag{30b}$$

Since $u^+ \geq 0$, and $u^- \leq 0$, f is a monotone function of its arguments $(\rho^n_{j-1}, \rho^n_j, \rho^n_{j+1})$ *iff* (29) is true.

Next since $\rho^0_j > 0, \forall j$, (30b) immediately gives

$$\rho^n_j > 0, \quad n > 0, \quad \forall j,$$

under the condition (29). Hence, the positivity of density is preserved. And (29) is called the *positivity condition.* The issue of preserving positivity of species mass fractions has also been studied by Larrouturou [24].

Remark: For linear case, $u_{j-1/2} = u_{j+1/2} = u$ =const., it is easy to show that (29) satisfies the TVD condition of Harten [25]. But for nonlinear case, condition (29) does not guarantee TVD.

Remark: Let

$$u^+_j = M^+_j a_{j+1/2}, \quad u^-_j = M^-_j a_{j-1/2}, \quad j \in Z, \tag{31a}$$

then we have the following inequality,

$$\left[u^+_{j+1/2} + (-u^-_{j-1/2})\right] \leq u^+_j - u^-_j. \tag{31b}$$

Proof. By definition,

$$\begin{aligned} 2u^+_{j+1/2} &= u_{j+1/2} + |u_{j+1/2}| = u^+_j + u^-_{j+1} + |u^+_j + u^-_{j+1}| \\ 2u^-_{j-1/2} &= u_{j-1/2} - |u_{j-1/2}| = u^+_{j-1} + u^-_j - |u^+_{j-1} + u^-_j| \end{aligned}$$

Then

$$\begin{aligned} 2(u^+_{j+1/2} - u^-_{j-1/2}) &= u^+_j + u^-_{j+1} - u^+_{j-1} - u^-_j + |u^+_j + u^-_{j+1}| + |u^+_{j-1} + u^-_j| \\ &\leq u^+_j + u^-_{j+1} - u^+_{j-1} - u^-_j + u^+_j - u^-_{j+1} + u^+_{j-1} - u^-_j \\ &= 2(u^+_j - u^-_j). \end{aligned}$$

Lemma 3.4: The above CFL-like positivity condition can be expressed in terms of a stronger condition for a given λ,

$$0 \leq \lambda \left[u_j^+ + (-u_j^-) \right] \leq 1. \tag{32}$$

Proof. Using (31), it is easy to see that (32) guarantees (29) for a given λ.

Comparison of Well Known Numerical Fluxes

Next, we write well-known numerical fluxes in a form similar to (28) for comparison.

Roe:

$$\mathbf{F}_{j+1/2} = \frac{1}{2}\left[(u\mathbf{\Phi})_j + (u\mathbf{\Phi})_{j+1} \right] - \frac{1}{2} \left| \mathbf{A}(\hat{\mathbf{U}})_{1/2} \right| \Delta_{j+1/2}\mathbf{U} + \frac{1}{2}(\mathbf{P}_j + \mathbf{P}_{j+1}), \tag{33a}$$

where $\hat{\mathbf{U}}$ is the Roe-averaged state, and $|\mathbf{A}| = \mathbf{A}^+ - \mathbf{A}^-$ in the usual sense.

Osher:

$$\mathbf{F}_{j+1/2} = \frac{1}{2}\left[(u\mathbf{\Phi})_j + (u\mathbf{\Phi})_{j+1} \right] - \frac{1}{2} \int_{\mathbf{U}_j}^{\mathbf{U}_{j+1}} |\mathbf{A}(\mathbf{U})| \, \mathbf{dU} + \frac{1}{2}(\mathbf{P}_j + \mathbf{P}_{j+1}). \tag{33b}$$

Steger-Warming:

$$\mathbf{F}_{j+1/2} = \frac{1}{2}\left[(u\mathbf{\Phi})_j + (u\mathbf{\Phi})_{j+1} \right] - \frac{1}{2} \Delta_{j+1/2}|\mathbf{A}|\mathbf{U} + \frac{1}{2}(\mathbf{P}_j + \mathbf{P}_{j+1}). \tag{33c}$$

Van Leer/Hänel:

$$\mathbf{F}_{j+1/2} = \frac{1}{2}\left[(M\mathbf{\Phi})_j + (M\mathbf{\Phi})_{j+1} \right] - \frac{1}{2} \Delta_{j+1/2}|M|\mathbf{\Phi} + \mathbf{P}_{j+1/2}. \tag{33d}$$

Remark: The Van Leer/Hänel splitting is seen also to require only $O(n)$ operations, since $|M|$ is a scalar.

Remark: The Steger-Warming and Roe splittings differ only in the evaluation of the absolute Jacobian. The absolute quantity in the latter is evaluated using *both* the "j" and "$j+1$" states and is taken *outside* of the difference operator. In fact, this comparison reveals clearly that a striking difference in form between the FVS and FDS lies in *whether the dissipation matrix (or scalar) is differenced.*

Remark: In the above sense, the present scheme may appear formally close to a FDS, but it differs in the averaged term. On the other hand, the method retains the efficiency of the

Van Leer scheme in defining the dissipation term. Moreover, it achieves the high level of accuracy attributed only to the Roe and Osher methods, as will be borne out by a variety of Euler and Navier-Stokes calculations. Consequently, the present scheme is neither FDS nor FVS, but rather a hybrid one.

Remark: It is of interest investigating the limiting form of the flux valid for the boundary layer flow where the transverse Mach number is small, $M_{1/2} << 1$. Assuming $M_{1/2} > 0$, the $y-$momentum flux (cf. (28)) becomes, by retaining only leading terms:

$$\mathbf{G}_{j+1/2} = \bar{M}\bar{\mathbf{\Phi}}(1-\frac{1}{2}\Delta_{j+1/2}M)-\frac{1}{2}\bar{M}(1-\frac{1}{2}\Delta_{j+1/2}M)\Delta\mathbf{\Phi}+\bar{\mathbf{P}}(1-\frac{3}{2}\Delta_{j+1/2}pM+\cdots), \quad (34)$$

where $\bar{f} = \frac{1}{2}(f_j + f_{j+1})$. Since the leading terms coincide with the central-difference approximation, the nominally first-order upwind formula (34) now tends to be second-order accurate as $M \to 0$.

Variants in Numerical Energy Flux

Furthermore, we propose another viable variation which we have found to be reliable. In the energy equation, the term (up) can be separated from the total flux $\rho u h_t$. Specifically, we suggest the following two options.

$$(\rho u h_t)_{j+1/2} = u^+_{j+1/2}\rho_j e_{tj} + u^-_{j+1/2}\rho_{j+1}e_{tj+1} + u_{j+1/2}p_{j+1/2}. \quad (35a)$$

The terms $u_{j+1/2}$ and $p_{j+1/2}$ are defined using (8b), (17), and (27).

Or following [22], we can derive

$$(\rho u h_t)_{j+1/2} = u^+_{j+1/2}\rho_j h_{tj} + u^-_{j+1/2}\rho_{j+1}h_{tj+1} + 4\sigma a^2_{j+1/2}(M^+_j M^-_j - M^-_{j+1}M^+_{j+1}), \quad (35b)$$

where the parameter σ gives reise a family of choices. As $\sigma = 0$, we recover the basic total-enthalpy-preserving scheme recommended in this paper. The original Van Leer splitting sets $\sigma = \frac{h}{2h+a^2}$. Note that the last parenthes in (35b) can take either positive or negative value although $M^-M^+ \leq 0$.

4. HIGHER-ORDER EXTENSION

While the first-order schemes are simple and useful for analysis, it is generally desirable to employ higher-order schemes. The extension, although aiming at improving accuracy, should as well preserve those properties arrived at for the first-order scheme, such as monotonicity, positivity, efficiency, and robustness. We will attempt to focus on these properties in this section.

The MUSCL [26] strategy for preserving monotonicity is adopted here, via the use of a nonlinear limiter sensing the ratio of neighboring first-differences of appropriate variables.

Many forms have been proposed in the literature and to our experiences they all work reasonably well although certain differences in computed results can exist. Systematic discussion on the subject of limiters is beyond the scope of this paper. We only give the formulas used in our calculations, acknowledging that there may be a more elaborate choice. In [21], we will address these issues in more detail.

Following the spirit of the present method that the fluxes can be evaluated sequentially, we avoid using the characteristic variables in the extrapolation procedure. It may suffice to extrapolate the primitive variables $\mathbf{W}$, thereby leading to a simple and efficient procedure:

$$\mathbf{W}_L := \mathbf{W}_j + \frac{1}{2}\psi(r_j)(\mathbf{W}_j - \mathbf{W}_{j-1}), \qquad \mathbf{W} = (\rho, u, p)^T,$$
$$\mathbf{W}_R := \mathbf{W}_{j+1} - \frac{1}{2}\psi(\frac{1}{r_{j+1}})(\mathbf{W}_{j+2} - \mathbf{W}_{j+1}), \tag{36}$$

where the subscripts "L" and "R" represent the states that take the place of "j" and "$j+1$" in the formulas derived in section 2 for the first-order scheme. To take grid nonuniformity into account, grid-size weighting can also be formulated into (36) if desired, see for example [27]. The function ψ is a limiter whose argument is defined as

$$r_j = \frac{\Delta_{j+1/2} w_i}{\Delta_{j-1/2} w_i}, \qquad \mathbf{W} = (w_1, w_2, w_3)^T = (\rho, u, p)^T. \tag{37}$$

The minmod and superbee functions are normally chosen in our calculations. The effects of limiters on either accuracy or convergence rate are often present, but discussion of them is beyond the scope of this paper. A note of suggestion may be warranted in the case of viscous calculations. For the reason of maintaining uniform accuracy and convergence rate, it is desirable that the limiters be set to unity insofar as stability is allowed, so that physically true extrema (such as the peak temperature in a thermal boundary) will not be clipped or the limit-cycle behavior can be minimized.

In what follows, we will show that the second-order scheme satisfies monotonicity and positivity conditions.

Let us again consider the continuity equation written in the finite-volume form (30a),

$$\rho_j^{n+1} = \rho_j^n - \lambda\Big(f^n_{\rho,j+1/2} - f^n_{\rho,j-1/2}\Big). \tag{30a}$$

Now we write the mass flux at "$j + 1/2$" as

$$f^n_{\rho,j+1/2} = u^+_{j+1/2}\rho^n_L + u^-_{j+1/2}\rho^n_R, \tag{38}$$

where, by virtue of (36),

$$\rho^n_L = \rho^n_j + \frac{1}{2}\psi^+_{j+1/2}(\rho^n_j - \rho^n_{j-1}) = \rho_L(\rho^n_{j-1}, \rho^n_j; \psi^+_{j+1/2}), \tag{39a}$$
$$\rho^n_R = \rho^n_{j+1} - \frac{1}{2}\psi^-_{j+1/2}(\rho^n_{j+2} - \rho^n_{j+1}) = \rho_R(\rho^n_{j+1}, \rho^n_{j+2}; \psi^-_{j+1/2}). \tag{39b}$$

In the above expression, we have adopted new notation for the limiters, for algebraic clarity.

$$\psi^+_{j+1/2} = \psi(r_j), \quad \psi^-_{j+1/2} = \psi(\frac{1}{r_{j+1}}). \tag{40}$$

Note that the superscripts "+" and "-" are used to associate them with forward and backward extrapolations, but without attaching sign values to them. Using (36), we express the limiters as

$$\psi^+_{j+1/2} = \psi^+_{j+1/2}(\rho^n_{j-1}, \rho^n_j, \rho^n_{j+1}), \qquad \psi^-_{j+1/2} = \psi^-_{j+1/2}(\rho^n_j, \rho^n_{j+1}, \rho^n_{j+2}), \tag{41}$$

and hence the interface densities as

$$\rho^n_L = \rho_L(\rho^n_{j-1}, \rho^n_j, \rho^n_{j+1}), \qquad \rho^n_R = \rho_R(\rho^n_j, \rho^n_{j+1}, \rho^n_{j+2}). \tag{42}$$

Similarly, we can write

$$u_{j+1/2} = u_{j+1/2}(u^n_{j-1}, u^n_j, u^n_{j+1}, u^n_{j+2}). \tag{43}$$

That is, we have a 5-point scheme in (30) as expected for the second-order method. By substitution,

$$\begin{aligned}\rho^{n+1}_j = \rho^n_j - \lambda\Big\{ & u^+_{j+1/2}\Big[\rho^n_j + \frac{1}{2}\psi^+_{j+1/2}(\rho^n_j - \rho^n_{j-1})\Big] + u^-_{j+1/2}\Big[\rho^n_{j+1} - \frac{1}{2}\psi^-_{j+1/2}(\rho^n_{j+2} - \rho^n_{j+1})\Big] \\ & - u^+_{j-1/2}\Big[\rho^n_{j-1} + \frac{1}{2}\psi^+_{j-1/2}(\rho^n_{j-1} - \rho^n_{j-2})\Big] - u^-_{j-1/2}\Big[\rho^n_j - \frac{1}{2}\psi^-_{j-1/2}(\rho^n_{j+1} - \rho^n_j)\Big]\Big\}.\end{aligned} \tag{44}$$

To utilize the simplicity found in the proof of **Lemma 3.3** for the first-order scheme, we first group the basic first-order terms, and then rearrange the remaining terms by utilizing (37), so that the resulting equation appears formally like the first-order scheme as in (30b).

After some algebraic manipulations, we get

$$\begin{aligned}\rho^{n+1}_j = \rho^n_j - \lambda\Big\{ & u^+_{j+1/2}\rho^n_j + u^-_{j+1/2}\rho^n_{j+1} - u^+_{j-1/2}\rho^n_{j-1} - u^-_{j-1/2}\rho^n_j\Big\} \\ & + \frac{\lambda}{2}\Big\{ - u^+_{j+1/2}\psi^+_{j+1/2}(\rho^n_j - \rho^n_{j-1}) + u^-_{j+1/2}\psi^-_{j+1/2}r_{j+1}(\rho^n_{j+1} - \rho^n_j) \\ & + u^+_{j-1/2}\frac{\psi^+_{j-1/2}}{r_{j-1}}(\rho^n_j - \rho^n_{j-1}) - u^-_{j-1/2}\psi^-_{j-1/2}r_{j+1}(\rho^n_{j+1} - \rho^n_j)\Big\}.\end{aligned}$$

Or

$$\rho^{n+1}_j = C_{j-1}\rho^n_{j-1} + C_j\rho^n_j + C_{j+1}\rho^n_{j+1}, \tag{45}$$

where

$$C_j = \left\{1 - \frac{\lambda}{2}\left[u^+_{j+1/2}(2+\psi^+_{j+1/2}) + (-u^-_{j-1/2})(2+\psi^-_{j-1/2}) \right.\right. \tag{46a}$$
$$\left.\left. + u^-_{j+1/2} r_{j+1}\psi^-_{j+1/2} - u^+_{j-1/2}\frac{\psi^+_{j-1/2}}{r_{j-1}}\right]\right\},$$

$$C_{j-1} = \frac{\lambda}{2}\left\{u^+_{j+1/2}\psi^+_{j+1/2} + u^+_{j-1/2}(2 - \frac{\psi^+_{j-1/2}}{r_{j-1}})\right\}, \tag{46b}$$

$$C_{j+1} = \frac{\lambda}{2}\left\{(-u^-_{j-1/2})\psi^-_{j-1/2} + (-u^-_{j+1/2})(2 - r_{j+1}\psi^-_{j+1/2})\right\}. \tag{46c}$$

Definition 4.1: The second-order accurate density function in (45) and (46) is monotone $\forall j$ and satifies the positivity condition $\forall n > 0$ *iff*

$$C_{j-1} \geq 0, \quad C_j \geq 0, \quad \text{and}, \quad C_{j+1} \geq 0, \quad j \in Z. \tag{47}$$

Let us define

$$u_{min} \leq u_{j-1/2},\ u_{j+1/2} \leq u_{max}, \quad \forall j, \tag{48}$$

and

$$u^+_{max} = \max\left[u_{max}, 0\right], \quad u^-_{min} = \min\left[u_{min}, 0\right]. \tag{49}$$

We turn now to show the conditions for the limiter function and a CFL-like inequality.

Lemma 4.1: Under the following conditions,

$$0 \leq \psi(r) \leq 2r \leq \psi_{max}, \tag{50}$$

and

$$\lambda(u^+_{max} - u^-_{min})(1 + \frac{\psi_{max}}{2}) \leq 1, \tag{51}$$

then (a) the density function is monotone, and (b) the scheme preserves positivity of density.

Proof. Since $u^+_{j\pm1/2} \geq 0$, and $u^-_{j\pm1/2} \leq 0$, and requiring

$$\psi^\pm_{j\pm1/2} \geq 0, \tag{52}$$

we have the following inequality,

$$C_{j-1} \geq \frac{u^+_{j-1/2}}{2}(2 - \frac{\psi^+_{j-1/2}}{r_{j-1}}),$$

and

$$C_{j+1} \geq \frac{-u^-_{j+1/2}}{2}(2 - r_{j+1}\psi^-_{j+1/2}).$$

This immediately yields that **Definition 4.1** (47) is met *iff*

$$\frac{\psi^+_{j-1/2}}{r_{j-1}} = \frac{\psi(r_{j-1})}{r_{j-1}} \leq 2, \tag{53a}$$

$$r_{j+1}\psi^-_{j+1/2} = r_{j+1}\psi(\frac{1}{r_{j+1}}) \leq 2, \tag{53b}$$

and

$$C_j = \left\{1 - \frac{\lambda}{2}\left[u^+_{j+1/2}(2 + \psi^+_{j+1/2}) + (-u^-_{j-1/2})(2 + \psi^-_{j-1/2}) \right.\right.$$
$$\left.\left. + u^-_{j+1/2}r_{j+1}\psi^-_{j+1/2} - u^+_{j-1/2}\frac{\psi^+_{j+1/2}}{r_{j+1}}\right]\right\} \geq 0. \tag{53c}$$

Using (48), (49), and (52), one can easily show

$$C_j \geq 1 - \frac{\lambda}{2}\left[u^+_{max}(2 + \psi^+_{j+1/2}) + (-u^-_{min})(2 + \psi^-_{j-1/2})\right].$$

Assuming $0 \leq \psi^{\pm}_{j\pm1/2} \leq \psi_{max}$, the above equation leads to

$$\lambda(u^+_{max} - u^-_{min})(1 + \frac{\psi_{max}}{2}) \leq 1.$$

This completes the proof of (a). The proof of (b) follows immediately as in **Lemma 3.3**.

Hence, we see that the positivity of density can be preserved from the "second-order (except at extrema)" scheme, (30a), (38), and (39) under conditions (50) and (51).

Remark: Similar proof can be found also in the TVD-type study. Also a weaker condition than (51) may be possible, e.g., by admitting $\psi \leq 0$, hence maintaining second-order accuracy at extrema. However, this is not the purpose of the above proof and is beyond the scope of the present paper.

5. GENERALIZED CURVILINEAR COORDINATES

This section gives a prescription for treating generalized curvilinear coordinates. To facilitate the description, let us first define the notation for the relevant variables in the 3D Euler equations. The physical variables in a phase space of dimension 5 are denoted

by a boldface uppercase letter or column vector whose elements are denoted by lowercase letters.

$$\mathbf{U} = \begin{pmatrix} \rho \\ \rho u \\ \rho v \\ \rho w \\ \rho e_t \end{pmatrix}, \quad \mathbf{\Phi} = \begin{pmatrix} \rho \\ \rho u \\ \rho v \\ \rho w \\ \rho h_t \end{pmatrix}, \tag{54}$$

where $e_t = e + 0.5(u^2 + v^2 + w^2)$ and $h_t = e_t + p/\rho$. The geometrical vectors in physical (Cartesian) space of dimension 3 are denoted by an overhead arrow "$\vec{\ }$". The fluid velocity is

$$\vec{V} = u\vec{i} + v\vec{j} + w\vec{k}, \tag{55a}$$

and the normal vector of the boundary surface of a control volume

$$\vec{S} = s_x\vec{i} + s_y\vec{j} + s_z\vec{k}. \tag{55b}$$

The inviscid fluxes in 3D physical space are compactly written as

$$\vec{\mathbf{F}} = \begin{pmatrix} \rho \\ \rho u \\ \rho v \\ \rho w \\ \rho h_t \end{pmatrix} \vec{V} + \begin{pmatrix} 0 \\ p\vec{i} \\ p\vec{j} \\ p\vec{k} \\ 0 \end{pmatrix} = \mathbf{\Phi}\vec{V} + \vec{\mathbf{P}} = \vec{\mathbf{F}}^{(c)} + \vec{\mathbf{P}}, \quad \text{where} \quad \vec{\mathbf{P}} = \begin{pmatrix} 0 \\ p\vec{i} \\ p\vec{j} \\ p\vec{k} \\ 0 \end{pmatrix}. \tag{56}$$

The first term in $\vec{\mathbf{F}}$ is the flux of $\mathbf{\Phi}$ convected by the fluid velocity $\vec{V}$ and the second term simply the pressure flux.

The inviscid conservation laws can be conveniently expressed over an arbitrary control volume Ω in an integral form:

$$\int_{\Omega} \frac{\partial \mathbf{U}}{\partial t} dv + \int_{\partial\Omega} [\mathbf{\Phi}\vec{V} + \vec{\mathbf{P}}] \bullet d\vec{S} = 0. \tag{57}$$

The discrete form, describing the rate of change of $\mathbf{U}$ in $v_{i,j,k}$ via balance of fluxes through all enclosing faces, $\vec{S}_l, l = 1, \cdots, LX(i,j,k)$, can be cast as

$$\mathbf{U}_{i,j,k}^{n+1} = \mathbf{U}_{i,j,k}^{n} - \frac{\Delta t}{v_{i,j,k}} \sum_{l=1}^{LX} (\vec{\mathbf{F}}_l^{(c)} + \vec{\mathbf{P}}_l) \bullet \vec{S}_l = 0. \tag{58}$$

In what follows, we give the algorithm for constructing the numerical fluxes in an arbitrary finite volume, based on that described in Section 2. Let us consider the situation in which the computation domain is divided into hexahedrons where each pair of opposing

faces constitute the coordinates ξ, η, and ζ with corresponding discrete indices i, j, and k, respectively. For the purpose of presenting the procedures, it suffices to consider one interface in the ξ-direction, whose surface vector is $\vec{S}^{\xi}_{i+1/2,j,k} = S_{i+1/2,j,k}\vec{n}_{\xi}$, $\vec{n}_{\xi}$ being the unit normal vector and $S_{i+1/2,j,k}$ the area. Again, we find it convenient to use the convention of the "L" and "R" states for representing conditions on each side of the interface $\vec{S}^{\xi}_{i+1/2,j,k}$.

(1) Project the velocity vector at the cell centers $(i,j,k),(i+1,j,k)$ to $\vec{S}^{\xi}_{i+1/2,j,k}$,

$$\tilde{V}_L = \vec{V}_{i,j,k} \bullet \vec{n}_{\xi}, \quad \tilde{V}_R = \vec{V}_{i+1,j,k} \bullet \vec{n}_{\xi}. \tag{59}$$

Hereinafter we use "overhead" $\tilde{(\ )}$ to denote quantities in curvilinear coordinates. It is reminded that if higher order accuracy is desired, extrapolation given in section 4 can be adopted for $\vec{V}_{i,j,k}$ and $\vec{V}_{i+1,j,k}$.

(2) Define the corresponding Mach numbers,

$$\tilde{M}_L = \frac{\tilde{V}_L}{a_{i+1/2,j,k}}, \quad \tilde{M}_R = \frac{\tilde{V}_R}{a_{i+1/2,j,k}}, \tag{60}$$

with a suitable definition of $a_{i+1/2,j,k}$ such as (27).

(3) Define the interface convective Mach number by writing

$$\tilde{M}_{i+1/2,j,k} = \tilde{M}^{+}_{L} + \tilde{M}^{-}_{R}, \tag{61}$$

where

$$\tilde{M}^{+}_{L} = \begin{cases} \frac{1}{2}(\tilde{M}_L + |\tilde{M}_L|), & \text{if } |\tilde{M}_L| \geq 1, \\ M^{+}_{\beta}(\tilde{M}_L), & \text{otherwise,} \end{cases} \quad \tilde{M}^{-}_{R} = \begin{cases} \frac{1}{2}(\tilde{M}_R - |\tilde{M}_R|), & \text{if } |\tilde{M}_R| \geq 1, \\ M^{-}_{\beta}(\tilde{M}_R), & \text{otherwise.} \end{cases}$$

The formulas for $M^{\pm}_{\beta}(M)$ are given in (14b).

(4) Obtain the interface pressure $p_{i+1/2,j,k}$ in a similar fashion by using the above-defined Mach numbers in (17)-(18),

$$\mathbf{P}_{i+1/2,j,k} = p_{i+1/2,j,k} \begin{pmatrix} 0 \\ n_{\xi_x} \\ n_{\xi_y} \\ n_{\xi_z} \\ 0 \end{pmatrix}_{i+1/2,j,k}. \tag{62}$$

(5) Assemble the interface numerical flux,

$$(\vec{\mathbf{F}} \bullet \vec{S})_{i+1/2,j,k} = \left\{ \tilde{M}^{+}_{i+1/2,j,k}\mathbf{\Phi}_{i,j,k} + \tilde{M}^{-}_{i+1/2,j,k}\mathbf{\Phi}_{i+1,j,k} + \mathbf{P}_{i+1/2,j,k} \right\} S_{i+1/2,j,k}. \tag{63}$$

Lemma 5.1: The CFL-like condition of the first-order scheme for the 3D case is

$$
\begin{aligned}
0 \le \frac{\Delta t}{v_{i,j,k}} [& (\tilde{V}^{+}_{i+1/2,j,k} S_{i+1/2,j,k} - \tilde{V}^{-}_{i-1/2,j,k} S_{i-1/2,j,k}) + \\
& (\tilde{V}^{+}_{i,j+1/2,k} S_{i,j+1/2,k} - \tilde{V}^{-}_{i,j-1/2,k} S_{i,j-1/2,k}) + \\
& (\tilde{V}^{+}_{i,j,k+1/2} S_{i,j,k+1/2} - \tilde{V}^{-}_{i,j,k-1/2} S_{i,j,k-1/2})] \le 1,
\end{aligned}
\tag{64}
$$

as the density satisfies the monotone condition and remains positive.

Proof. The proof directly follows that in **Lemma 3.3.**

Remark: A similar formula for the second-order accurate scheme also can be derived, see **Lemma 4.1.**

6. BOUNDARY CONDITIONS

This topic generally does not get enough space in a paper. From an analytical point of view, the boundary conditions required to close the mathematical system are well defined. When these analytical boundary conditions are transformed in the numerical discretization, ambiguities and difficulties begin to compound with the interior flux schemes. While a number of papers have been devoted to proposing and analyzing numerical boundary conditions, unfortunately this issue still has not received sufficient investigation. Often it is barely mentioned in a paper, and the exact implementation, where variations begin, is generally left out. The situation is even more disappointing in the case of unsteady flows.

We also assert that there is a tight relation between the interior scheme and the selection of apppropriate boundary conditions. In other words, the concern of compatibility between a numerical flux scheme and boundary scheme must be observed – a numerical boundary procedure working properly for scheme A may not be suitable for scheme B. To our knowledge, little has been reported on this aspect.

Of various types of boundary conditions, the treatment at a physical wall (solid or porous) perhaps is one of the most diverse among CFD practitioners, and is the one that affects solution behavior (accuracy and convergence rate) the most if due care is not exercised. Although this situation has been observed, to sort out the issues involved is beyond the scope of the present paper. Nevertheless, we give in the following the procedures used for inviscid solid wall conditions, on which all comparisons among methods are based.

A linear extrapolation of all variables from the nearest interior points (two points in the case of second-order solution) to the wall is employed. For slip wall, we impose the condition of zero velocity component normal to the wall to recover the Cartesian components. In Fig. 4, we let

$$
\vec{V}_{ex} = \vec{V}_1 + \frac{l_1}{l_2}(\vec{V}_1 - \vec{V}_2),
$$

and

$$V_n = \vec{V}_{ex} \cdot \vec{n}_w.$$

Then a simple vector relation yields

$$\vec{V}_w = \vec{V}_{ex} - V_n \vec{n}_w. \tag{65}$$

As a result, the inviscid numerical flux is simply

$$\mathbf{F}_w = \vec{\mathbf{F}}_w \bullet \vec{n}_w = \begin{pmatrix} 0 \\ p_w n_{wx} \\ p_w n_{wy} \\ p_w n_{wz} \\ 0 \end{pmatrix}, \tag{66}$$

where p_w is extrapolated from interior point(s).

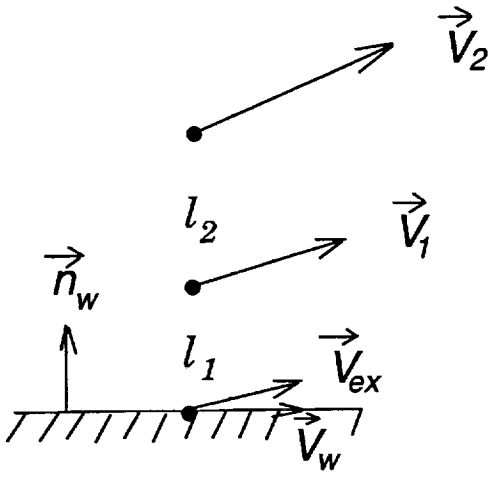

Fig. 4 Wall boundary condition.

7. RESULTS AND DISCUSSION

In this section we demonstrate the capability of the proposed numerical flux by confirming the mathematical consequences established in previous sections for various relevant problems. The problems are listed below and will be discussed accordingly.

1. Stationary shock discontinuity,
2. Stationary contact discontinuity,
3. Hypersonic conical boundary layer,
4. 1D shock tube problems,

5. 2D channel flow,
6. Blunt body flow,
7. Odd-even grid perturbation problem,
8. Shock diffraction around a corner.

For validation purposes, analytical solutions will be used as much as they are available. Otherwise, solution will be compared with that obtained by using Roe's splitting as it has been established as an accurate and perhaps the most popular upwind scheme in use today.

The first three problems are 1D steady flows, dealing with the capability of accurately resolving shock, contact discontinuity, and a thin viscous layer; the last one of these tends in the limit of $Re \to \infty$ to behave as a contact discontinuity. In problems 4, we are concerned with accuracy in calculating unsteady flows. In problems 5 and 6, we consider 2D steady inviscid flows. Finally, 2D unsteady solutions are discussed in problems 7 and 8.

In some problems, first-order solution is included. Test on first-order solution is very meaningful for it reveals the sheer accuracy of a scheme, and the monotonicity. It is also fundamental because the TVD schemes and higher-order solutions can be built up from the first-order scheme.

Figures 5 and 6, respectively, show the numerical result for a single stationary shock and contact discontinuity. The present AUSM$^+$, like Roe splitting, is designed specifically to produce exact solution in these cases. In contrast, the AUSM and Van Leer splittings resolve the shock with two intermediate points. As mentioned earlier, a specific choice of speed of sound (Eq. (25) or (27)) used in the Van Leer splitting can also yield an exact shock solution. Unfortunately, this modification is not sufficient to rescue the Van Leer splitting from producing "fatty" dissipation in the limit of vanished flow speed. Figure 6 shows that both Roe and AUSM$^+$ (also AUSM) splittings give rise to exact solution of a stationary discontinuity, while the Van Leer splitting increasingly smears the discontinuity as calculation continues.

The quasi-1D conical flow at $M_\infty = 7.95$ over a cone of 10° half angle was calculated using 64 cells. The profiles of pressure, temperature, and transverse velocity component on 64 cells are shown in Fig. 7 for the first-order results and in Fig. 8 the second-order results. The Roe splitting and the AUSM$^+$ give nearly identical results; interestingly the convergence rates also show remarkable resemblance. It is noted that the first-order result is already as good as the second-order one. To further raise curiosity, we include a first-order coarse-grid (32 cells) result of AUSM$^+$ for comparison; the accuracy is astonishing in that there are only about four (4) cells for resolving the extremely high-gradient boundary layer and the shock is nearly captured exactly. Roe solution behaves identically but is not included for the sake of clarity in plots.

Next we consider the standard shock-tube problems. Here we used 100 cells and the minmod limiter for the "second-order" calculation. The CFL number was set 0.45. For the Sod problem, Fig. 9 clearly demonstrates the comparable accuracy of the present and the

Roe solution. The second-order solution shown in Fig. 10 again confirms the accuracy. We also add the more difficult problems studied by Yee [28], corresponding roughly to cases C and E in [28] in terms of density and pressure ratios and initial Mach number except without chemistry effects. The former involves a much stronger contact discontinuity than the Sod problem; the latter has a shock moving slowly against a high pressure region, with characteristics similar to that studied by Roberts [29], and with an additional large density jump. Figure 11 begins to show the differences between results obtained using the AUSM$^+$ and Roe splitting. Immediately behind the shock, the AUSM$^+$ appears to give better agreement with the exact solution of velocity. In Fig. 12, a long wave oscillation of the Roe solution, observed by Roberts [29] and Lin [30], also appears in this problem. Both AUSM$^+$ and AUSM results seem to be free from this behavior, but AUSM gives rise a glitch in the solution due to a large gradient at the contact discontinuity.

We turn now to 2D calculations. First we show, in Fig. 13, the Mach contours of an $M = 1.8$ flow over a 15° ramp. We used the minmod limiter and CFL=0.8 on 138×38 cells. The ramp shock is sufficiently strong so that a Mach reflection appears on the top wall. A similar but weaker Mach stem also shows up on the bottom wall. In both cases, a distinct shear layer emanating from the triple point can be seen. Detailed distributions along the top and bottom walls are dispalyed in Figs. 14 and 15, among AUSM, AUSM$^+$, and Roe solutions; they essentially agree with each other, results by AUSM and AUSM$^+$ nearly indistinguishable. The convergence history in Fig. 16 in terms of L_2 norm exhibits that the Roe solution stalls after having dropped about three orders, while the other two residuals continue to decrease, also with nearly identical pace. We stress that the presented solutions have been confirmed to be grid-independent, hence the fine-grid solutions are not included.

Second case in this category is a standard 4% bump in a channel with $M_\infty = 1.4$. The results were obtained using 132×68 cells, minmod limiter, and CFL=0.9. Again, the profiles on the bump wall in Fig. 17 show that three solutions agree well and all give sharp representation of three shocks, two respectively located at the leading and trailing edge of the bump and one located further downstream and produced by the reflection of the leading-edge shock from the other wall. The convergence history of the Roe solution behaves similarly to the previous case, as displayed in Fig. 18, except that it stalls at a much lower level. The AUSM and AUSM$^+$, however, continue to behave well.

Let us now consider a supersonic $M_\infty = 6.0$ flow over a circular cylinder. This seemingly benign problem in fact fails the Osher and Roe methods [21,30]. The so-called "carbuncle" phenomenon by Roe's method is exhibited in front of the cylinder, as compared with the AUSM$^+$ result in Fig. 19. Figure 20 displays the solutions by AUSM and AUSM$^+$, showing a crisp shock resolution at the centerline. In particular, the AUSM$^+$ exhibits the evidence of improvement over the AUSM by eliminating the post-shock overshoot and almost getting rid of numerical shock point. Figure 21 compares the convergence history of various solutions, showing the effects of order of spatial accuracy, grid size, and CFL number. It is surprising to see that the second-order method in fact converges faster than

the first-order method, even with the shock. Finer grid makes the convergence slower, as consistent with other published results.

Next, we study a very interesting and benign problem, first reported by Quirk [4]. A plane shock is moving into a quiescent region in a long constant-area channel. The computation grid is perturbed at the centerline by a very small magnitude, $\pm 10^{-6}$ in our case, alternately at odd and even points. The Roe solution, seen in Fig. 22(a), quickly develops an odd-even decoupling behavior, eventually leading to an unacceptable solution. The present method, on the other hand, still preserves the plane shock even after a long time, as shown in Fig. 22(b). The variables profiles along the centerline, corresponding to the contours, are displayed in Fig. 23 for comparison — the AUSM$^+$ gives monotone and well behaved solution.

The last problem is the diffraction of a supersonic moving shock over a 90-degree bend and the resulting complex flowfield. Quirk [4] has painstakingly shown the complexity of the flow using grid refinement to resolve the fine details. He pointed out that there was some numerical difficulty encountered in the use of the Roe splitting. Thus it would be an interesting problem to test whether the present AUSM$^+$ would have the same difficulty or even face another. First we show the density contours of first-order AUSM$^+$, Roe, and Godunov solutions on a 71×71 grid, † which is extremely coarse for revealing any intricacy. Nevertheless, it confirms the findings of Woodward and Collela [31] and Quirk [4] that the Godunov scheme, as formally extended to 2D in the same manner as the other schemes reported in the present paper, can yield discontinuous expansion fans as seen in Fig. 24(a) — this, apparently violating entropy condition, clearly causes concern. Figures 24(b) and 24(c) show that both the AUSM$^+$ and Roe splittings respectively are able to break the expansion fans, while the AUSM$^+$ solution appears to have slightly more diverged fans than the Roe solution. A fine grid (400×400) calculation was made using minmod limiter and CFL=0.4. The result is depicted in Fig. 25. The intricacy associated with this flow is astonishingly rich, although what is contained at this grid resolution is still not nearly comparable to that captured by Quirk [4].

8. CONCLUDING REMARKS

In this paper we presented the construction and analysis of a new numerical flux scheme — AUSM$^+$. We gave the associated mathematical properties and proved its monotonicity, positivity, and CFL-like condition. We proposed a modification to the Mach number and pressure polynomials used in the AUSM. Furthermore, a judicious choice of numerical speed of sound for the interface Mach number was shown to give exact resolution for an 1D steady shock and significantly improved shock resolution in 2D cases. The reliability of the new scheme was evident as well in calculating some unsteady problems that

† These results were obtained with the generosity of Dr. Yasuhiro Wada who kindly provided his code for producing not only solution but also plots.

have failed prominent flux schemes. We also stress that in addition to the demonstrated accuracy and reliability, the AUSM$^+$ requires computational effort far less than the flux difference splittings and only insignificantly more than Van Leer's flux vector splitting. Moreover, since an exact linearization of the AUSM$^+$ flux can be derived, a consistent implicit scheme using these Jacobians is available. Results on this aspect will be reported in the near future.

ACKNOWLEDGMENT

It has been a very rewarding experience for the author working with Dr. Yasuhiro Wada who spent a year at ICOMP, NASA Lewis Research Center, on leave from NAL of Japan. The author thanks Dr. Erlunder Steithorsson of ICOMP for providing comments to improve the paper.

References

1. M.-S. Liou, and C. J. Steffen, Jr., "A New Flux Splitting Scheme," *J. Comput. Phys.* **107**, 23 (1993).
2. M.-S. Liou, "On a New Class of Flux Splittings," *Lecture Notes in Physics* **414**, 115 (1993).
3. P. L. Roe, "A Survey of Upwind Differencing Techniques," *Lecture Notes in Physics* **323**, 69 (1989).
4. J. J. Quirk, "A Contribution to the Great Riemann Solver Debate," ICASE Report 92-64, 1992.
5. J. L. Steger, and Warming, R. F., "Flux Vector Splitting of the Inviscid Gasdynamics Equations with Application to Finite Difference Methods," *J. Comput. Phys.* **40**, 263 (1981).
6. B. van Leer, "Flux-Vector Splitting for the Euler Equations," *Lecture Notes in Physics* **170**, 507 (1982).
7. B. van Leer, J. L. Thomas, P. L. Roe, and R. W. Newsome, 8th AIAA CFD Conference, AIAA Paper 87-1104CP, 1987.
8. M.-S. Liou and C. J. Steffen, Jr., "High-Order Polynomial Expansions (HOPE) for Flux-Vector Splitting," NASA TM 104452, 1991.
9. P. L. Roe, "Approximate Riemann Solvers, Parameter Vectors and Difference Schemes," *J. Comput. Phys.* **43**, 357 (1981).
10. S. Osher and F. Solomon, "Upwind Difference Schemes for Hyperbolic Systems of Conservation Laws," *Math. Comp.* **38**, 339 (1982).
11. Y. Wada and M.-S. Liou, "A Flux Splitting Scheme with High-Resolution and Robustness for Discontinuities," AIAA 94-0083.
12. F. Coquel and M.-S. Liou, "Stable and Low Diffusive Hybrid Upwind Splitting Methods," Proceedings of the First European Computational Fluid Dynamics Conference, Vol. 1, pp. 9-16, 1992.
13. F. Coquel and M.-S. Liou, "Field by Field Hybrid Upwind Splitting Methods," 11th AIAA CFD Conference, AIAA paper 93-3302-CP, 1993.
14. F. Coquel and M.-S. Liou, NASA TM (to appear).
15. D. Hänel, R. Schwane, and G. Seider, "On the Accuracy of Upwind Schemes for the Solution of the Navier-Stokes Equations," 8th AIAA CFD Conference, AIAA paper 87-1105-CP, 1987.
16. D. Hänel and R. Schwane, "An Implicit Flux-Vector Splitting Scheme for the Computation of Viscous Hypersonic Flow," AIAA Paper 89-0274, 1989.
17. B. van Leer, "Flux-Vector Splitting for the 1990s," NASA CP-3078, p.203, 1991.
18. A. Jameson, "Artificial Diffusion, Upwind Biasing, Limiters and their Effect on Accuracy and Multigrid Convergence in Transonic and Hypersonic Flows," 11th AIAA CFD Conference, AIAA Paper 93-3359, 1993.

19. D. W. Halt and R. K. Agarwal, "A Novel Algorithm for the Solution of Compressible Euler Equations in Wave/Particle Split (WPS) Form," 11th AIAA CFD Conference, Open Forum Paper, 1993.
20. J. L. Steger, "Coefficient Matrices for Implicit Finite Difference Solution of the Inviscid Fluid Conservation Law Equations," *Comput. Methods Appl. Mech & Eng.* **13** 175 (1978).
21. M.-S. Liou and Y. Wada, "A Critical Study of Numerical Schemes for Solving Fluid Equations," (in preparation).
22. M.-S. Liou, B. van Leer, and J.-S. Shuen, "Splitting of Inviscid Fluxes for Real Gases," *J. Comput. Phys.* **87,** 1 (1990).
23. J. A. Owczarek, *Fundamentals of Gas Dynamics,* International Textbook Co., Scranton, Pennsylvania, 1964. 1972.
24. B. Larrouturou, "How to Preserve the Mass Fractions Positivity when Computing Compressible Multi-Component Flows," *J. Comput. Phys.* **95,** 59 (1991).
25. A. Harten, "A High Resolution Scheme for the Computation of Weak Solutions of Hyperbolic Conservation Laws," *J. Comput. Phys.* **49,** 357 (1983).
26. B. van Leer, "Towards the Ultimate Conservation Difference Scheme, V, A Second-Order Sequel to Godunov's Method," *J. Comput. Phys.* **32,** 101 (1979).
27. Liou, M.-S., and Hsu, A. T. "A Time Accurate Finite Volume High Resolution Scheme for Three Dimensional Navier-Stokes Equations," 9th AIAA CFD Conference, AIAA paper 89-1994-CP, 1989.
28. H. C. Yee, "Upwind and Symmetric Shock-Capturing Schemes," NASA TM 89464, 1987.
29. T. W. Roberts, "The behavior of Flux Difference Splitting Schemes near Slowly Moving Shock Waves," *J. Comput. Phys.* **90,** 141 (1990).
30. K. M. Peery and S. T. Imlay, "Blunt-Body Flow Simulations," AIAA paper 88-2904, AIAA/SAE/ASME/ASEE 24th Joint Propulsion Conference, 1988.
31. P. R. Woodward and P. Collela, "The Numerical Simulation of Two-Dimensional Fluid Flow with Strong Shocks," *J. Comput. Phys.* **54,** 115 (1984).

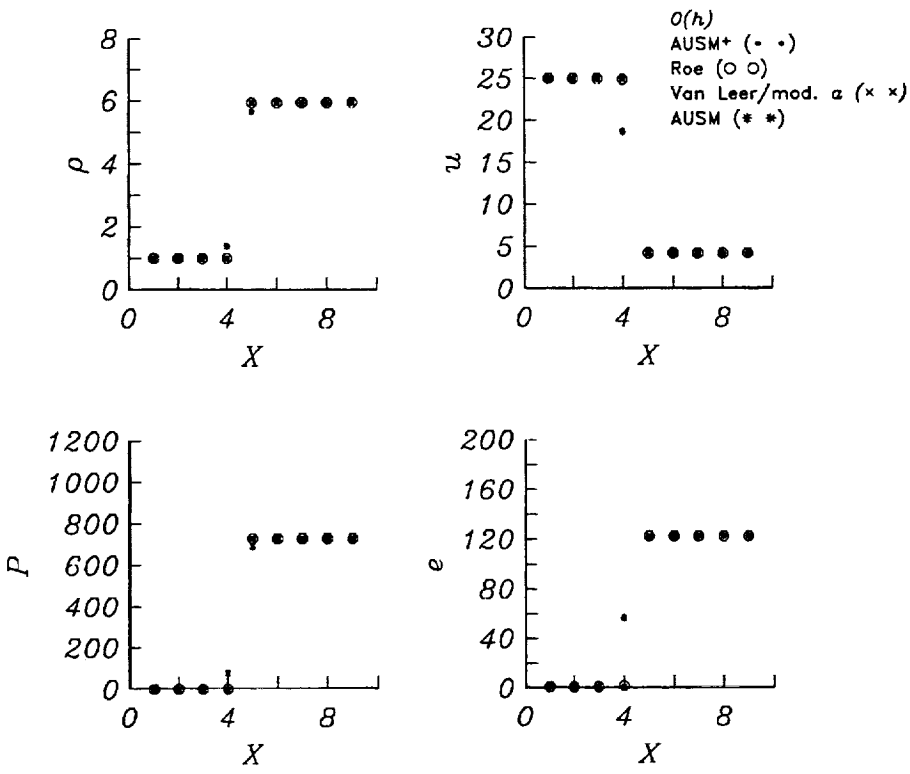

Fig. 5 Stationary shock discontinuity.

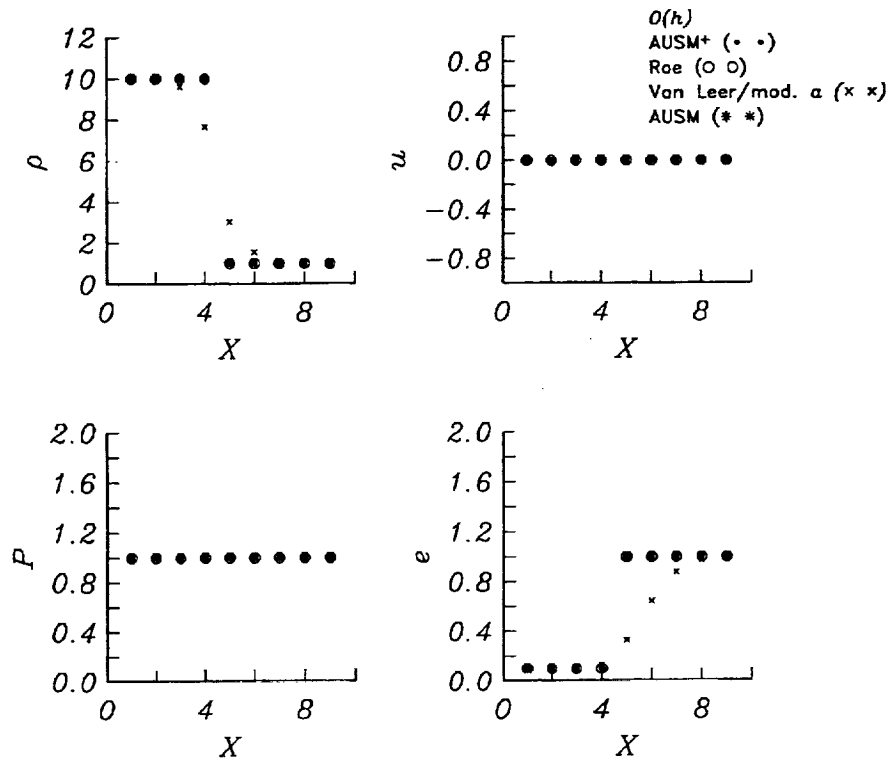

Fig. 6 Stationary contact discontinuity.

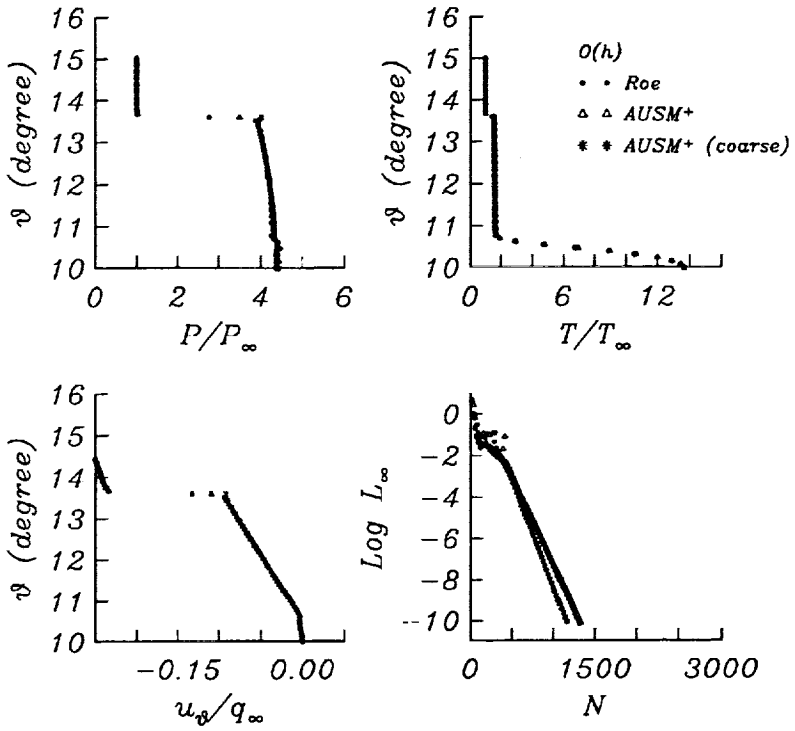

Fig. 7 Hypersonic conic flow; first-order solution.

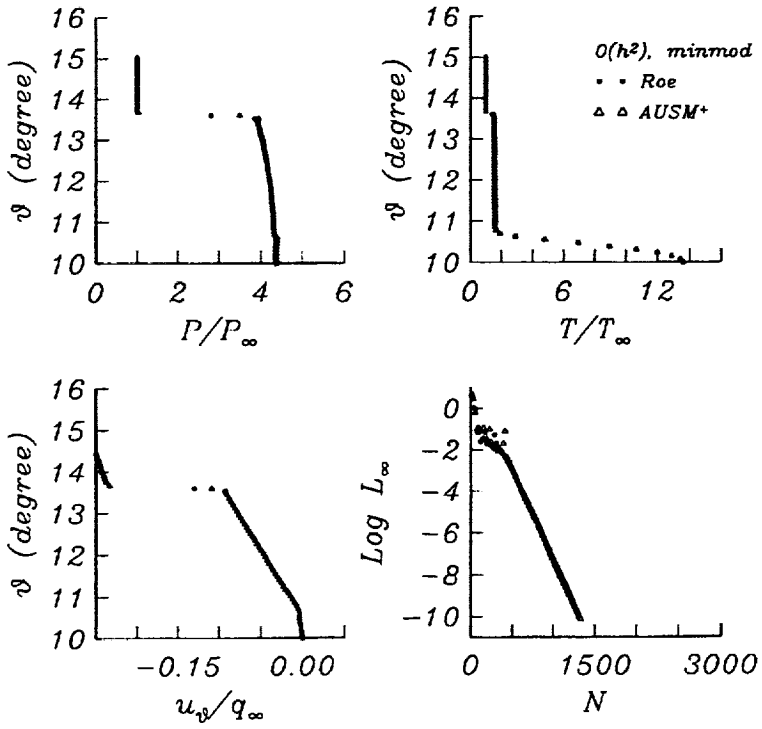

Fig. 8 Hypersonic conic flow; second-order solution.

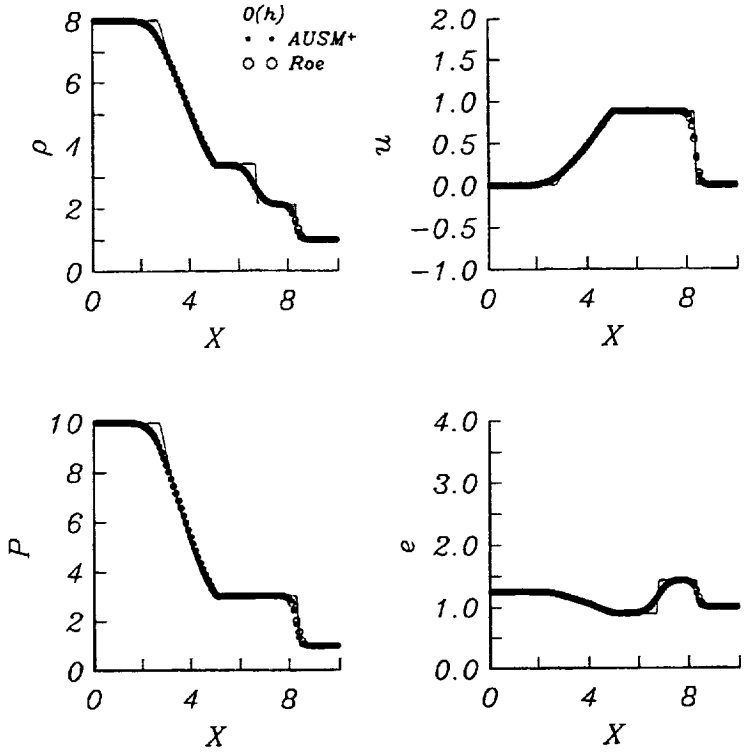

Fig. 9 Sod problem; first-order solution.

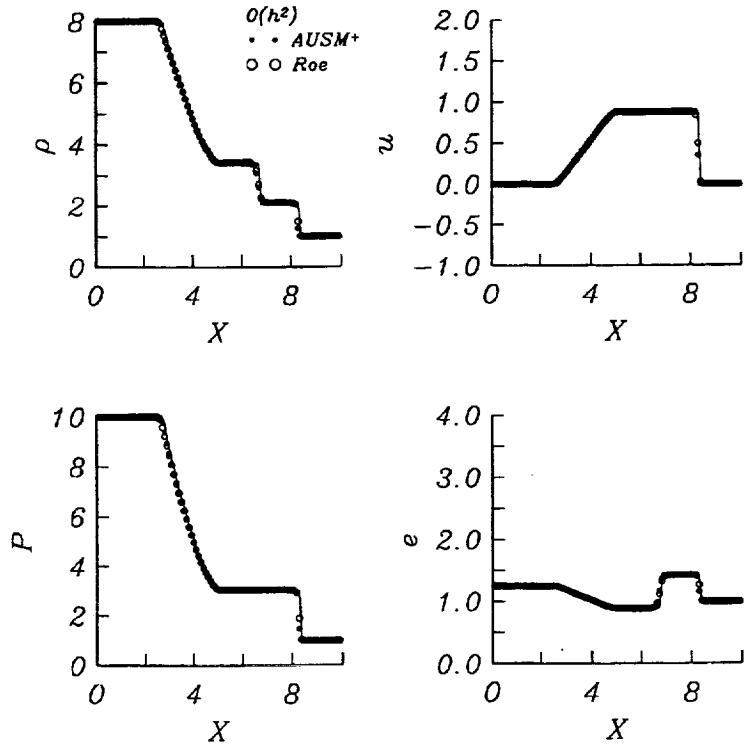

Fig. 10 Sod problem; second-order solution.

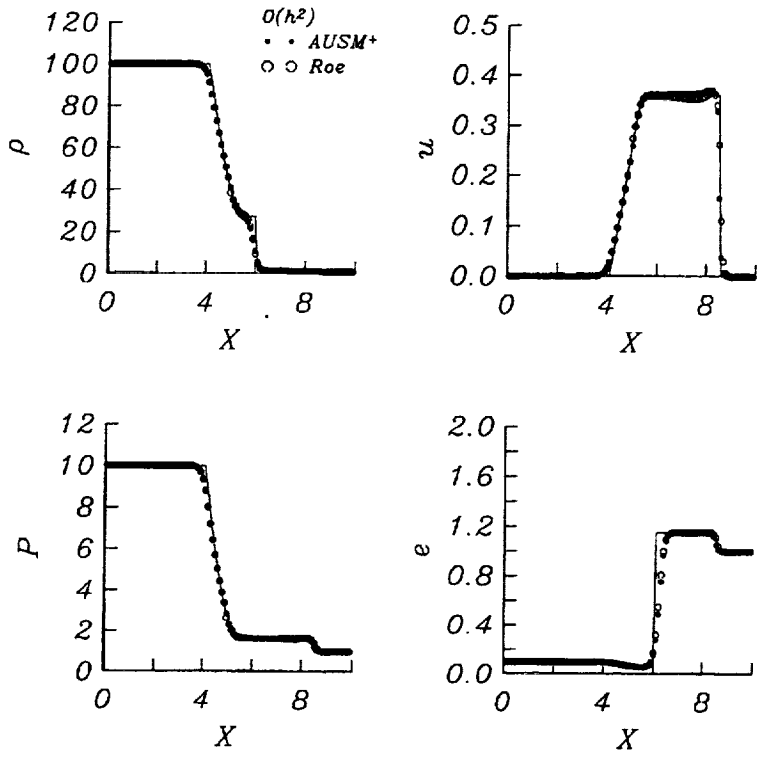

Fig. 11 Problem C; second-order solution.

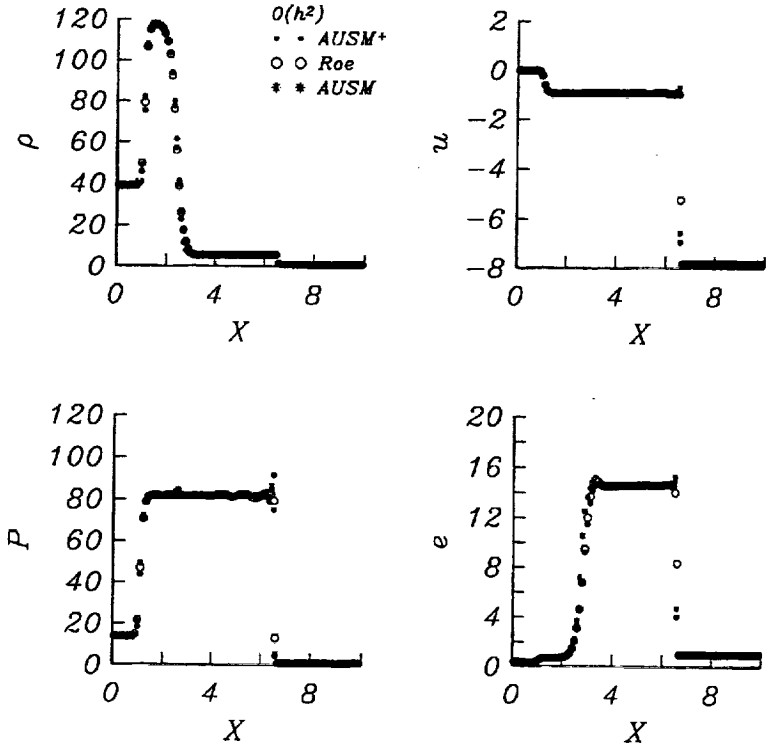

Fig. 12 Problem E; second-order solution.

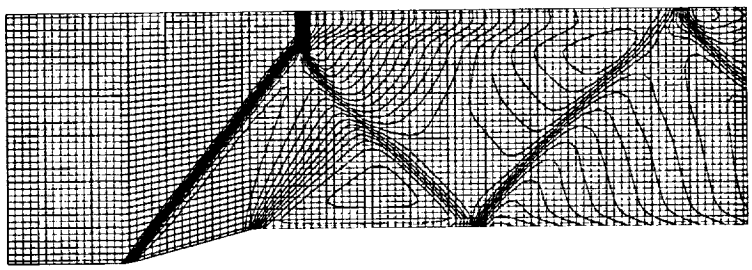

Fig. 13 Supersonic ramp problem; Mach number contours.

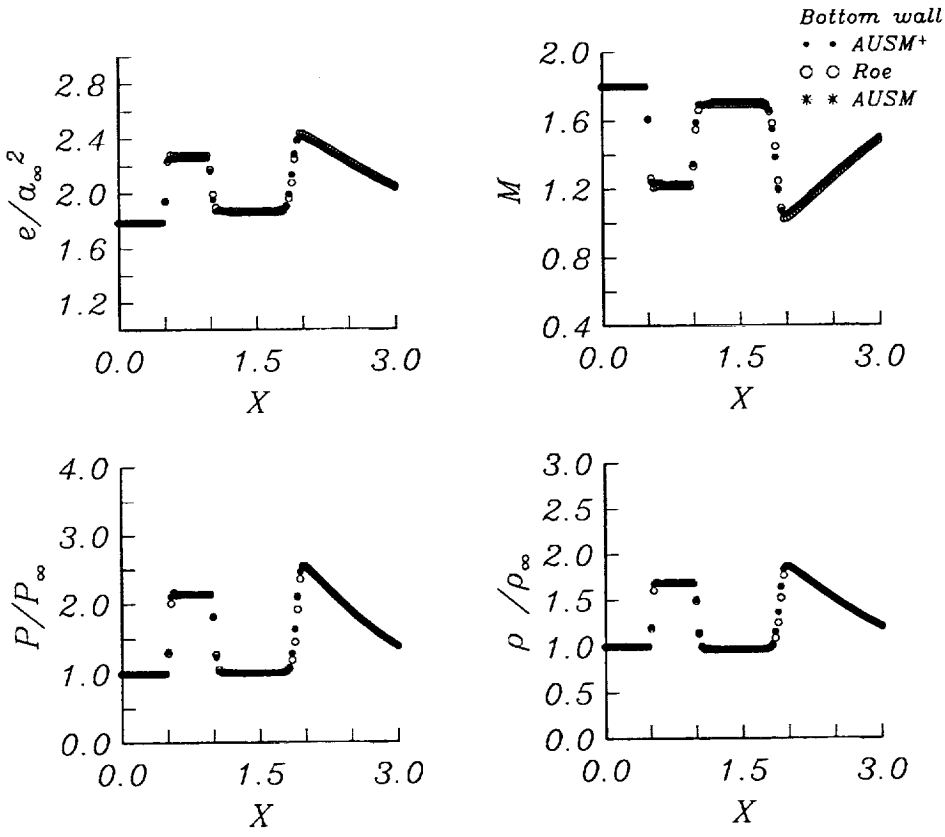

Fig. 14 Supersonic ramp problem; profiles on bottom wall.

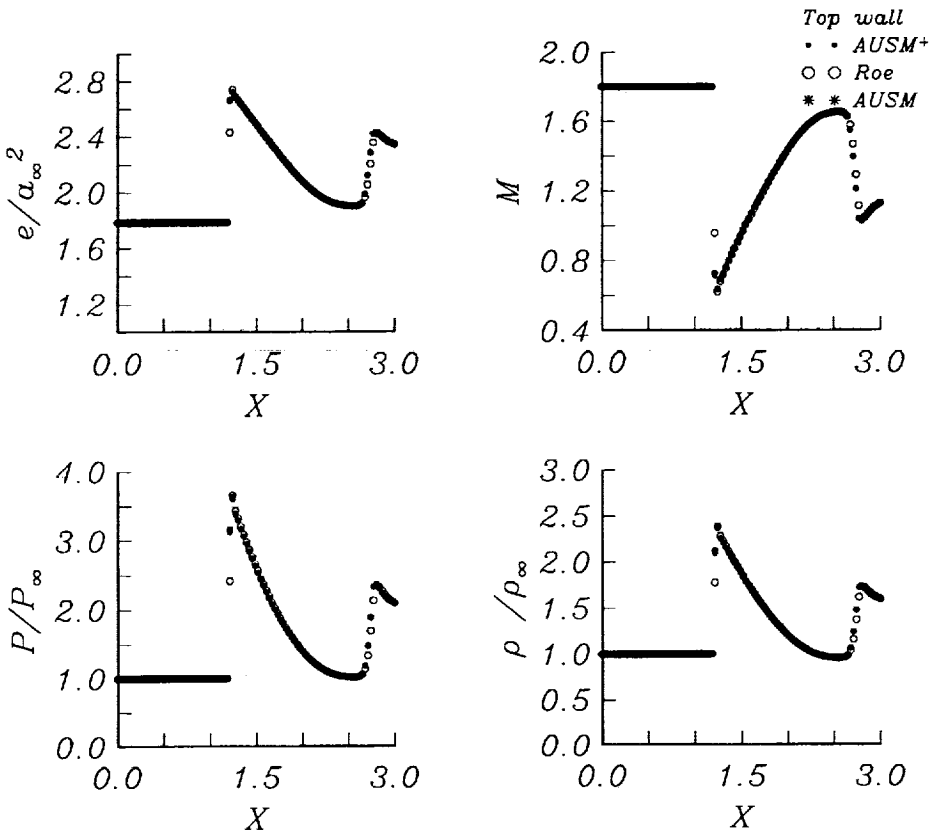

Fig. 15 Supersonic ramp problem; profiles on top wall.

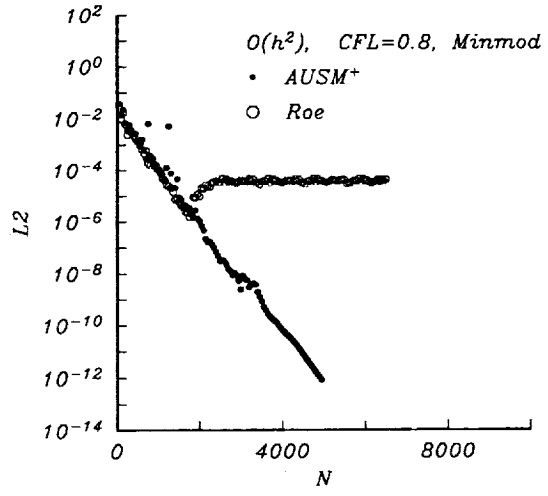

Fig. 16 Convergence history for supersonic ramp problem; second-order solution.

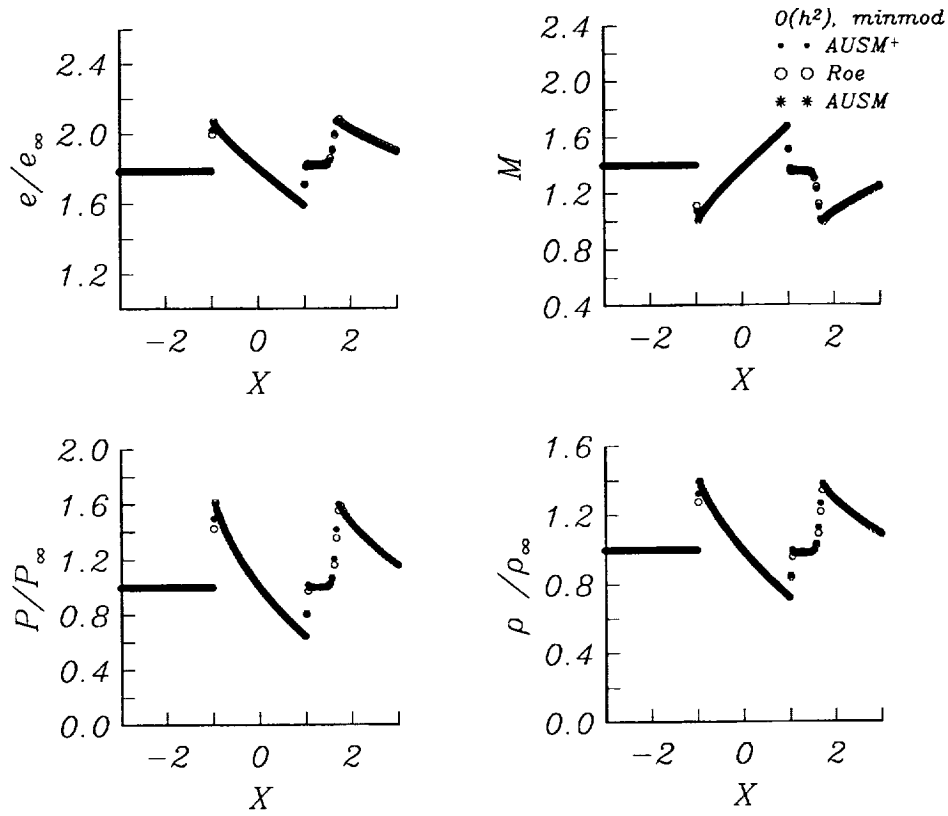

Fig. 17 4% bump problem; second-order solution on the bump.

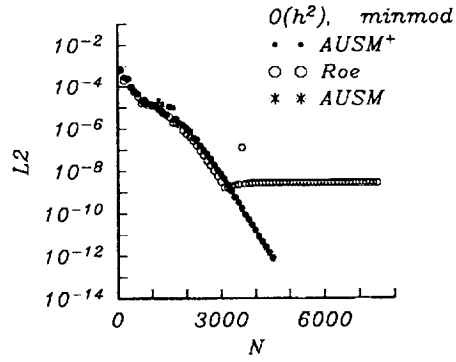

Fig. 18 Convergence history for 4% bump problem; second-order solution.

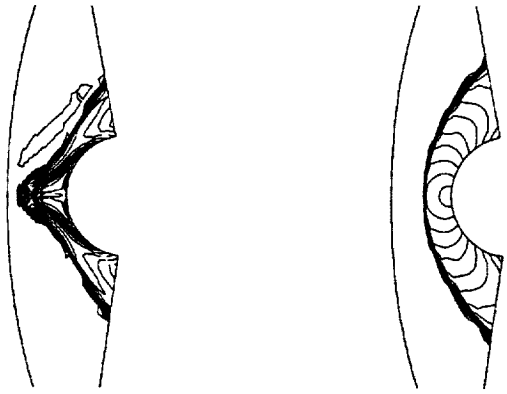

Fig. 19 Supersonic blunt body problem; Mach contours, left: Roe method, right: AUSM$^+$.

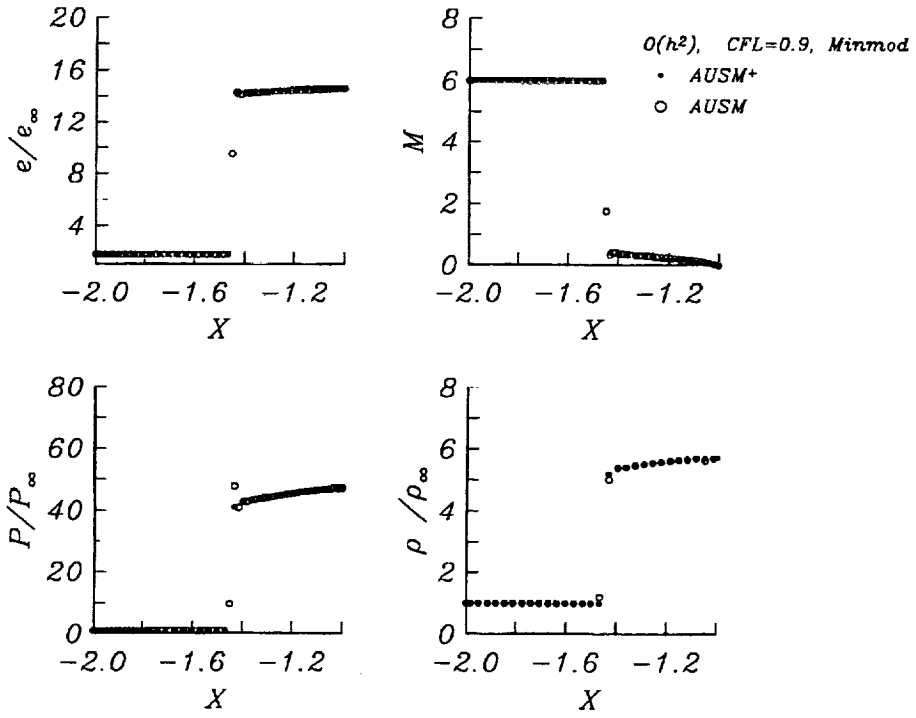

Fig. 20 Supersonic blunt body problem; second-order solution.

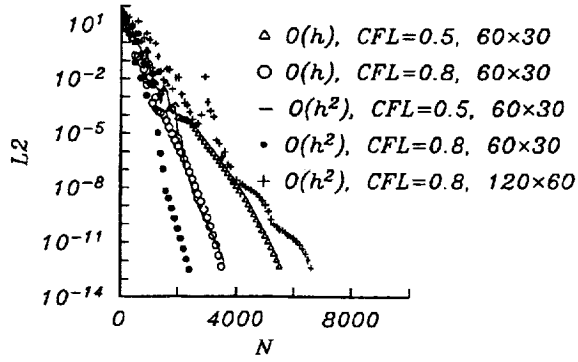

Fig. 21 Convergence history for supersonic blunt body problem.

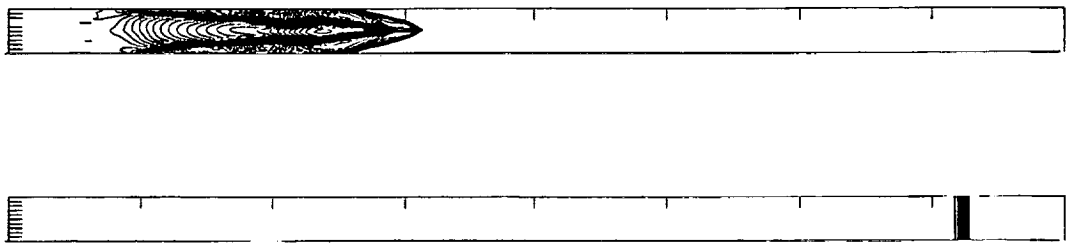

Fig. 22 Odd-even gird perturbation problem; Mach contours, top: Roe method, bottom: AUSM$^+$.

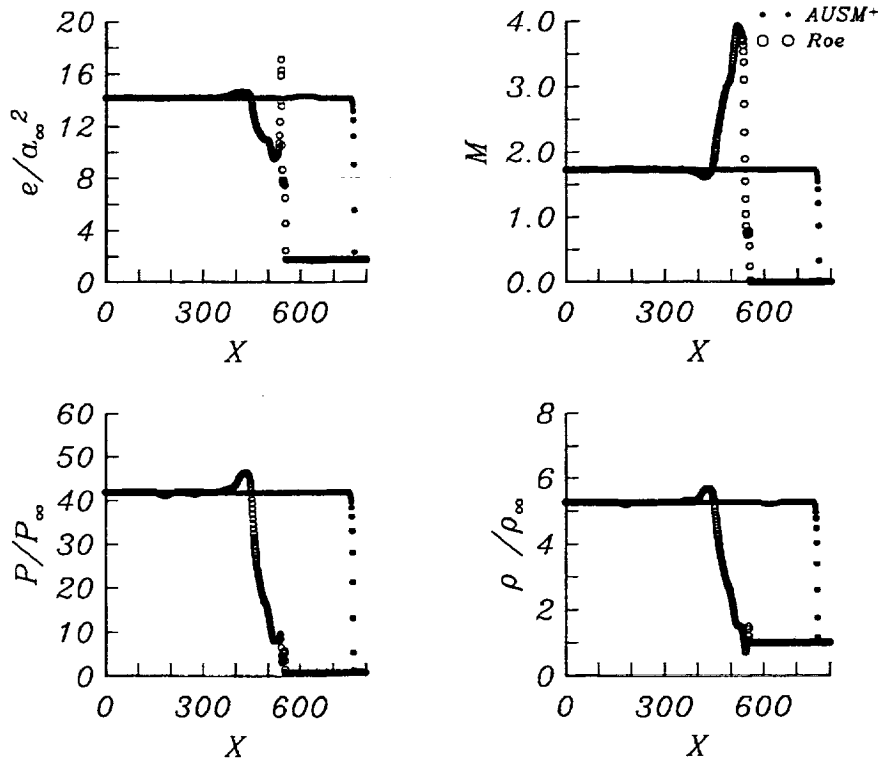

Fig. 23 Odd-even gird perturbation problem; profiles along the centerline.

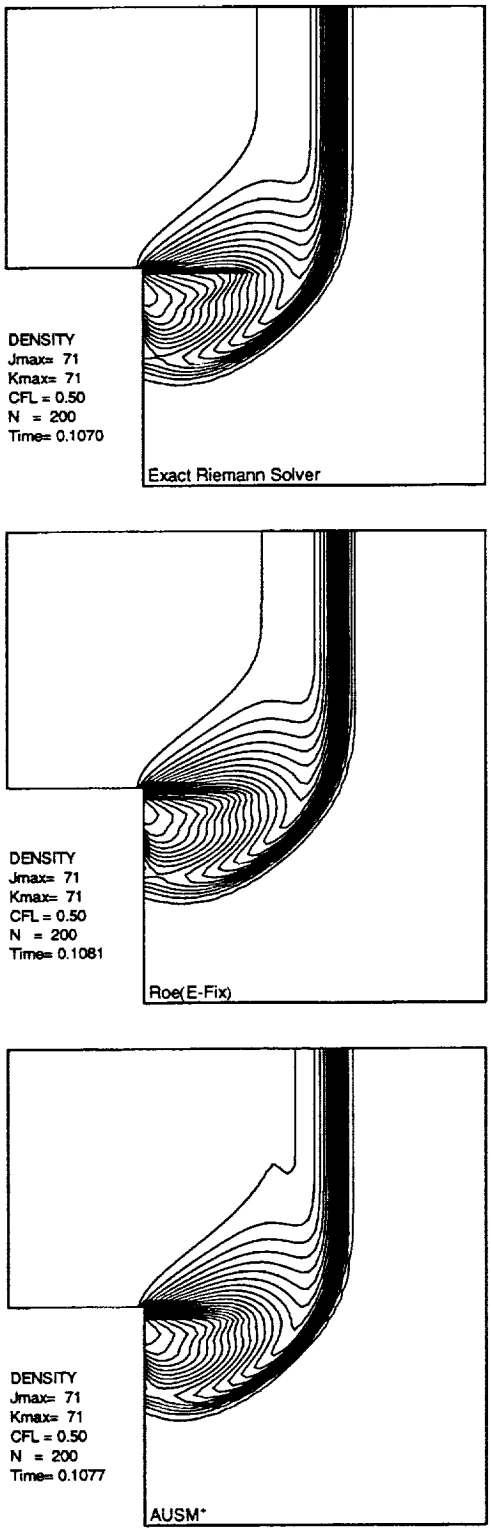

Fig. 24 Supersonic corner flow problem; density contours of first-order solution, top: Gudonov method, middle: Roe method, bottom: AUSM$^+$.

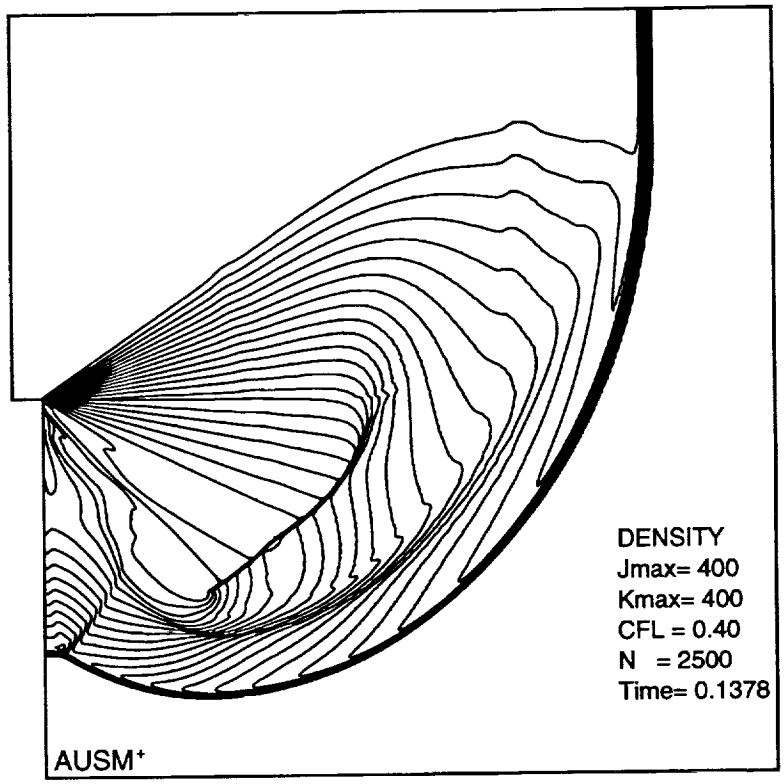

Fig. 25 Supersonic corner flow problem; density contours of second-order (minmod limiter) AUSM$^+$ solution on 400×400 grid.

REPORT DOCUMENTATION PAGE

Form Approved
OMB No. 0704-0188

1. AGENCY USE ONLY (*Leave blank*)	2. REPORT DATE	3. REPORT TYPE AND DATES COVERED
	March 1994	Technical Memorandum

4. TITLE AND SUBTITLE
A Continuing Search for a Near-Perfect Numerical Flux Scheme
Part I: AUSM+

5. FUNDING NUMBERS
WU-505-62-52

6. AUTHOR(S)
Meng-Sing Liou

7. PERFORMING ORGANIZATION NAME(S) AND ADDRESS(ES)
National Aeronautics and Space Administration
Lewis Research Center
Cleveland, Ohio 44135-3191

8. PERFORMING ORGANIZATION REPORT NUMBER
NASA TM-106524

9. SPONSORING/MONITORING AGENCY NAME(S) AND ADDRESS(ES)
National Aeronautics and Space Administration
Washington, D.C. 20546-0001

10. SPONSORING/MONITORING AGENCY REPORT NUMBER

11. SUPPLEMENTARY NOTES
A brief version of this paper was presented as an invited paper at the 5th International Symposium on Computational Fluid Dynamics, Sendai, Japan, August 31–September 3, 1993. Responsible person, Meng-Sing Liou, organization code 2600, (216) 433–5855.

12a. DISTRIBUTION/AVAILABILITY STATEMENT
Unclassified - Unlimited
Subject Categories 02, 34, and 64

12b. DISTRIBUTION CODE

13. ABSTRACT (*Maximum 200 words*)

While enjoying demonstrated improvement in accuracy, efficiency, and robustness over existing schemes, the Advection Upstream Splitting Scheme (AUSM)[1,2] has been found to have some deficiencies in extreme cases. This paper describes recent progress towards improving the AUSM while retaining its advantageous features. The new scheme, termed AUSTM+, features: (1) Unification of velocity and Mach number splitting reported in [1,2], (2) Exact capture of a single stationary shock, and (3) Improvement in accuracy. In this paper, we lay out a general construction of the ASUSM+ scheme and then focus on the analysis of the a scheme and its mathematical properties, heretofore unreported. We prove monotonicity and positivity, and give a CFL-like condition, for first and second order schemes and for generalized curvilinear co-ordinates. Finally, results of numerical tests on many problems are given to confirm the capability and improvements on a variety of problems including those failed by prominent schemes.

14. SUBJECT TERMS
Upwind flux; Euler and Navier-Stokes equations; Steady and unsteady flows; Positivity

15. NUMBER OF PAGES
47

16. PRICE CODE
A03

17. SECURITY CLASSIFICATION OF REPORT	18. SECURITY CLASSIFICATION OF THIS PAGE	19. SECURITY CLASSIFICATION OF ABSTRACT	20. LIMITATION OF ABSTRACT
Unclassified	Unclassified	Unclassified	